CUKUROVA UNIVERSITY
INSTITUTE OF NATURAL AND APPLIED SCIENCES

MSc THESIS

Investigating the Performance of a PV-Driven VRF System Using Cold Thermal Storage in Mediterranean Climate

Ahmad ITANI

Mechanical Engineering Department

August 2023

CUKUROVA UNIVERSITY
INSTITUTE OF NATURAL AND APPLIED SCIENCES

MSc THESIS APPROVAL

Investigating the Performance of a PV-Driven VRF System Using Cold Thermal Storage in Mediterranean Climate

---

Ahmad ITANI

Mechanical Engineering Department

This Master's Thesis was evaluated by the following Jury Members on 28/08/2023 and was approved by unanimity / majority of votes.

Jury : Prof. Dr. Hüseyin AKILLI (Advisor) ……………………

: Assist. Prof. Dr. Engin PINAR ……………………

: Assoc. Prof. Dr. Fırat EKİNCİ ……………………

This Thesis was written in the Department of Mechanical Engineering, Institute of Natural and Applied Sciences.

Thesis Number:

Prof. Dr. Sadık DİNÇER
Director
Institute of Natural and Applied Sciences

CONTENTS

CUKUROVA UNIVERSITY
INSTITUTE OF NATURAL AND APPLIED SCIENCES

MSc THESIS

Investigating the Performance of a PV-Driven VRF System Using Cold Thermal Storage in Mediterranean Climate

Ahmad ITANI

Advisor: Prof. Dr. Hüseyin AKILLI

Department of Mechanical Engineering

ABSTRACT

The demand for cooling has surged due to rising global temperatures, prompting interest in solar cooling systems categorized as electrically driven and thermally driven. Thermally driven systems employ solar thermal collectors and absorption chillers for cooling, constrained to a 20-ton minimum capacity and requiring backup heating or electric cooling without solar energy. Electrically driven systems, powered by photovoltaic panels, suit existing air conditioning and smaller cooling setups. This study examines a photovoltaic solar electrical-driven variable refrigerant flow system paired with cold phase change material thermal storage, targeting nearly zero-energy cooling in a 300m² Adana villa. Using the "Design Builder" program, baseline and optimized energy models were built, adhering to Turkish Thermal Insulation Requirements. Models were compared for year-round cooling energy rates. The challenge of storage led to investigating cost-effective cold thermal storage, countering short-lived costly batteries with reduced initial expenses and load-shifting. The research aims to optimize PV panel area and electrical/thermal storage using the "Hooke and Jeeves" technique.

Keywords: Solar Driven, VRF, Cooling Energy, Phase Change, Energy Storage.

ÇUKUROVA ÜNİVERSİTESİ
FEN BİLİMLERİ ENSTİTÜSÜ

YÜKSEK LİSANS TEZİ

Akdeniz İkliminde Soğuk Termal Depolama Kullanarak PV Destekli VRF Sisteminin Performansının İncelenmesi

Ahmad ITANI

Danışman: Prof. Dr. Hüseyin AKILLI

Makine Mühendisliği Anabilim Dalı

ÖZ

Soğutma talebi, artan küresel sıcaklıklar nedeniyle arttı ve elektrikle çalışan ve termal olarak tahrik edilen güneş soğutma sistemlerine olan ilgiyi artırdı. Termal tahrikli sistemler, soğutma için minimum 20 ton kapasiteyle sınırlandırılmış ve güneş enerjisi olmadan yedek ısıtma veya elektrikli soğutma gerektiren güneş termal toplayıcıları ve emme soğutucuları kullanır. Fotovoltaik panellerle çalışan elektrikle çalışan sistemler, mevcut klimaya ve daha küçük soğutma kurulumlarına uygundur. Bu çalışma, 300m ² Adana villada neredeyse sıfır enerji soğutmayı hedefleyen, soğuk faz değişim malzemesi termal depolama ile eşleştirilmiş bir fotovoltaik güneş enerjili elektrikle çalışan değişken soğutucu akışkan akış sistemini inceliyor. "Tasarım Oluşturucu" programı kullanılarak, Türk Termal Yalıtım (TS825) Gereksinimlerine uygun olarak temel ve optimize edilmiş enerji modelleri oluşturulmuştur. Modeller yıl boyunca soğutma enerji oranları için karşılaştırıldı. Depolama zorluğu, düşük maliyetli soğuk termal depolamanın araştırılmasına, kısa ömürlü maliyetli pillerin azaltılmış başlangıç giderleri ve yük değişimi ile karşılanmasına yol açtı.

Anahtar Kelimeler: Güneş Enerjili, VRF, Faz Değişimli, Enerji Depolama, TS825.

GENİŞLETİLMİŞ ÖZET

Küresel nüfusun ve kentsel altyapının hızla genişlemesi, enerji talebinde endişe verici bir artışa yol açmıştır. Özellikle bina sektörü, işletme ve inşaatıyla birlikte dünya nihai enerji tüketiminin üçte birinden fazlasını oluşturan önemli bir katkı sağlamıştır. Bu durum, yüksek verimli ve aynı zamanda CO2 emisyonlarından yoksun olan klima sistemlerinin geliştirilmesinin baskın bir gereklilik olduğunu vurgulamaktadır. Bu aciliyet, artan klima ihtiyacının yol açtığı sera gazı emisyonlarındaki artışla daha da kötüleşmektedir. Bu zorluklar arasında güneş enerjisi, geleneksel fosil yakıt tüketimine alternatif olarak giderek daha fazla ilgi görmektedir. Güneş enerjili soğutma teknolojilerinin daha erişilebilir fiyat noktalarında sunulmaya başlanması, bu alandaki dikkate değer bir gelişmedir. Bu teknolojiler arasında, fotovoltaik güneş sistemleri ve VRF (değişken soğutucu akış) sistemleri, enerji tüketimini etkili bir şekilde azaltmalarıyla öne çıkmaktadır. Güneş termal kazanımını kullanır ve kurutucu soğutma mekanizmalarını değerlendirirken koşullandırılmış hava sağlamak için kullanırlar, kapsamlı bir çözüm sunarlar. Bu güneş enerjili sistemlerin cazibesi, küresel ölçekte farklı ısıtma ve soğutma uygulamalarına uzanmaktadır. Soğutma çözümlerine olan artan talep, artan termal yükler, gelişen konfor beklentileri ve mimari tercih değişiklikleri gibi faktörlerden kaynaklanmaktadır. Güneş enerjili sistemler, bu trendlere uyumlu, enerji verimli çözümler sunarak, nüfus artışı, kentselleşme ve ardından gelen klima talebi ile ilişkilendirilen artan enerji gereksinimlerini karşılama vaadi taşıyan çözümler sunarlar.

Araştırma, Adana Şehri'nin Türkiye'nin güney bölgesinde yer alan yerel bir temel villa (LBV) üzerinde odaklanmaktadır. Bu villa, TS 825 Türk Binalarda Isı Yalıtımı Gereksinimlerine uygun olarak inşa edilmiştir. İlk adımlar, villa'nın ısı dengesini ve soğutma talep yükünü belirleyerek sistem boyutlarını tespit etmeyi içerir. Parametrik bir çalışma, enerji azaltma üzerindeki geliştirmelerin etkilerini incelemekte ve optimize edilmiş villa (OPV) için saatlik termal enerji profillerini şekillendirmektedir. Design Builder kullanılarak, izolasyon, aktiviteler, oda düzenleri ve bölgesel hava verileri gibi bina özellikleri entegre edildi. Bu yaklaşım, Design Builder'ın simülasyonlarından yıllık saatlik soğutma talebini çıkarmada yardımcı oldu. Bu çalışmanın ayrıntılı bina modellerinin, parametrik analizin ve simülasyonların entegrasyonu, villanın enerji performansını artırmayı amaçlamaktadır. Elde edilen görüşler, enerji verimliliğini artırma ve soğutma taleplerini azaltma potansiyeli taşımakta olup, bölgede sürdürülebilir yapı uygulamalarına ve enerji koruma çabalarına değerli katkılarda bulunmaktadır.

Soğutma talebinin gece saatlerinde etkin bir şekilde ele alınabilmesi için, çalışma iki ayrı depolama çözümünün geliştirilmesini önermektedir. İlk çözüm, fazladan üretilen enerjinin gündüz saatlerinde yakalanıp elektrik enerjisi olarak depolandığı elektrikli bataryaların kullanımını içermektedir. Bu depolanan enerji daha sonra gece boyunca değişken soğutucu akış (VRF) ünitesini çalıştırmak için kullanılarak sürekli ve enerji verimli bir soğutma işlemi

sağlanmaktadır. İkinci depolama mekanizması, Faz Değişim Malzemesi'nin (PCM) uygulanması etrafında dönüyor. Bu yenilikçi yaklaşım, enerjinin termal latent enerji olarak depolanmasını içermektedir. Bu depolanan enerji daha sonra hem gündüz hem de gece boyunca serbest bırakılarak sürekli bir soğutma sağlanmasını kolaylaştırmaktadır. Bununla birlikte, elektrikli bataryalar etkili bir enerji depolama çözümü sunsa da genellikle daha yüksek maliyetlerle ilişkilendirilir. Ayrıca, termal depolamanın soğutma döngüsüne entegre edilmesi, enerji dönüşümü ve transferindeki verimsizlikler nedeniyle enerji kayıplarına yol açabilir. Bu zorlukları göz önünde bulundurarak, çalışma PCM'yi içeren özgün bir enerji depolama stratejisinin gerekliliğini vurgular. Bu strateji, PV enerji üretiminin avantajları ile VRF sisteminin gereksinimleri arasında denge kurmayı amaçlar. PCM'nin bu bağlamda dikkatlice entegrasyonunu araştırarak ve optimize ederek, geleneksel enerji depolama yöntemlerinin ortaya koyduğu sınırlamaların üstesinden gelmeyi ve enerji üretimi, depolama ve kullanımı arasında daha sorunsuz ve verimli bir senkronizasyon elde etmeyi amaçlar.

Ana amaç, her bir model içindeki iki kurulu sistemden yıl boyunca sürekli bir soğutma yükü sağlamaktır; bu, genel hedefle uyumlu bir biçimde gerçekleştirilmektedir. Ancak, bu görev keşfedilmesi gereken çok sayıda potansiyel yöntem ve olasılığı içerir. Kapsamlı bir keşfi kolaylaştırmak amacıyla, "Visual Basic" yazılımı kullanılarak kullanıcı dostu bir arayüz programı geliştirilmiştir. Hooke ve Jeeves Yöntemi kullanılarak, bir Termo-Ekonomik Optimizasyon çerçevesi programa entegre edilmiştir. Bu optimizasyon süreci, üretilen çıktıları dinamik olarak girdi parametrelerini ayarlamak için kullanmaktadır. Bu yaklaşım aracılığıyla, çalışma, her bir sistemin en iyi konfigürasyonunu belirlemeyi ve böylece ekonomik ve termodinamik faktörleri göz önünde bulundurarak arz ve talep arasında istenen dengeyi sağlamayı amaçlamaktadır.

Bir tam yıl boyunca gerçekleştirilen ayrıntılı saatlik geçici simülasyonlar etkileyici içgörüler sunar. Göz önünde bulundurulan çeşitli işletim programları arasında, Değişken Soğutucu Akış (VRF) sisteminin 24 saat sürekli çalışması, "OPV" olarak kısaltılan, hem ilk kurulum maliyetleri hem de devam eden işletme giderleri açısından en tercih edilen seçenek olarak öne çıkmaktadır. Bu özel sistem konfigürasyonu, enerji tüketimini azaltma ve çevresel etkiyi kısıtlama kapasitesini dikkate değer şekilde göstermektedir. Performans metriklerini dikkatle incelediğimizde, "OPV" sisteminin yıllık elektrik tüketiminde %9'a kadar önemli bir azalmayı başarma yeteneğine sahip olduğu açıkça ortaya çıkmaktadır. Ayrıca, bu artan verimlilik çevresel faydalara da uzanır, çünkü "OPV" sistemi, karbondioksit emisyonlarında belirgin bir azalmaya katkı sağlayarak potansiyelini sergiler. Özetlemek gerekirse, saatlik simülasyonlardan elde edilen bulgular, 24 saatlik VRF sisteminin, "OPV"nin işletme kabiliyetini vurgular. Sadece ekonomik geçerlilik açısından düşük maliyetlerle öne çıkmakla kalmaz, aynı zamanda enerji tüketimini ve karbon ayak izini belirgin şekilde azaltma kapasitesinde de üstün performans sergiler; bu da geleneksel bölgesel termal santral modeli "LBV" üzerine önemli bir ilerlemeyi temsil eder.

Yapılan olasılık analizleri, önerilen sistemin avantajlarını vurgulamaktadır. Temel modelde, PV-PCM sistemi, PV-Batteries alternatifine kıyasla %27.41 oranında önemli bir maliyet tasarrufu sağladı. Buna ek olarak, geri ödeme süresinde %23'lük bir azalma ve dikkate değer %33.6 oranında bir İç Oranı Getirisi (IRR) artışıyla desteklendi. Optimize edilmiş modelde, PV-PCM sistemi PV-Batteries alternatifine kıyasla daha ekonomik ve karlı olduğunu sürdürüyor. %24.4 daha düşük yatırım maliyetine sahip olması, geri ödeme süresinin %27.3 daha kısa olması ve dikkate değer %32.3 yüksek IRR'si ile öne çıkıyor. Bu bulgular, PV-PCM sisteminin finansal yeteneğini vurgulayarak, hem temel senaryoda hem de optimize edilmiş senaryoda çekici ve avantajlı bir seçenek olduğunu göstermektedir.

Enerji koruma ve verimlilik önlemlerini benimseyerek, optimize edilmiş model, özellikle PV-Batteries sistemi bağlamında, yerel temel değerlere uygun olan "LBV" sistemi ile karşılaştırıldığında dikkate değer iyileştirmeler sergiliyor. Özellikle, optimize edilmiş model, enerji kullanımının düzenlenmiş olduğunu gösteren %11 daha az PV panel gerektiriyor. Ek olarak, gereken batarya depolama kapasitesi %10 azalıyor ve verim kazancını vurguluyor. Bu da sırasıyla yatırım maliyetlerinde %8.3'lük etkileyici bir azalmaya ve dikkate değer %5.2'lik geri ödeme süresinin azalmasına yol açıyor. Optimize edilmiş modelin üstünlüğünü daha da vurgulayan bir diğer nokta, İç Oran Getirisi (IRR) ve karlılık endeksinde temel modelle karşılaştırıldığında %8.2'lik bir artıştır. Faydalar PV-PCM sistemi için de geçerlidir. Bu bağlamda, optimize edilmiş model, gereken PV panel sayısında %11.5'lik önemli bir azalma ve PCM depolama kapasitesinde %6.3'lük bir azalma yaşar, bu da rafine edilmiş enerji kullanımını gösterir. Optimize edilmiş model aynı zamanda %3.07'lik bir yatırım maliyeti azalması, geri ödeme süresinde %8.8'lik bir artışla birlikte geldi—bu artan verimliliğin bir kanıtıdır. Dahası, IRR önemli bir %7.7 artış alır, bu da optimize edilmiş modelin iyileştirilmiş finansal uygunluğunu yansıtır. Bu, karlılık endeksinde %8.1'lik bir artış ile desteklenir, böylece ekonomik cazibesinin artırıldığını vurgular. Toplu olarak, bu bulgular optimize edilmiş model içinde enerji verimli stratejileri benimsemenin dönüştürücü etkisini vurgular; temel modelle karşılaştırıldığında çeşitli parametrelerde önemli kazançlar elde edilir.

ACKNOWLEDGEMENTS

The past year has been a challenging one on a personal level, it was a year full of tests and challenges. From saying goodbye to my family leaving behind my country and my surroundings and moving to Türkiye to building a career and a future and being a master's student at Çukurova University. However, I am grateful to all these challenges as they are the reason behind the new version of myself.

This research becomes a reality with the kind support and the help of many individuals to whom I would like to extend my sincere thanks.

I would like to express my sincere gratitude to whom supported me during the period of my Masters. My foremost gratitude goes toward my principal supervisor, Prof. Dr. Hüseyin AKILLI for the continuous support of my master's study and research, motivation, enthusiasm, and immense knowledge. I also wish to extend my sincere appreciation to the committee members for their invaluable support and great advice.

I gratefully acknowledge Çukurova University, not only for providing a scholarship for my master's degree, which allowed me to undertake this research, but also for giving me the opportunity to develop my teaching and learning skills.

I would also like to express my sincere gratitude towards Türkiye Burslari (YTB) for granting me a scholarship for studying in one of the prestigious universities in Türkiye.

Special thanks to my lovely family, for their constant encouragement and support in my whole life. Words cannot express how grateful I am to my mother, and father for all the sacrifices that they have made on my behalf.

LIST OF TABLES

TABLE OF FIGURES

SYMBOLS AND ABBREVIATIONS

VRF	: Variable Refrigerant Flow
CPCM	: Cold phase Change Material
$Q_{discharged,e}$	: The electric energy that could possibly be discharged from the storage
$Q_{electric,needed:}$	: Hourly electric energy rate needed for VRF, Design Builder (kWh)
$Q_{charged,e}$	: The electric energy that could be charged in the storage
Q_{PCM}	: Maximum charging capacity of PCM tank (kWh)
CTES	: Cold thermal energy storage
G*dn*	: hourly direct normal solar irradiance
G*diff*	: hourly diffuse horizontal solar irradiance
MPPT	: Maximum power point tracking
ACF	: Actual cash flow at year
COP	: Coefficient of performance
OPV	: Optimized villa
LBV	: Local baseline villa
TWH	: Terawatt hours
IRR	: Internal rate of return
$\eta_{storage}$	: Efficiency of PCM storage
$Q_{cooling,available}$	: Cooling energy hourly rate which produced from the VRF unit
$Q_{cooling,needed}$	: Cooling hourly energy rate calculated Design Builder
$Q_{difference}$	: Difference hourly rate between the cooling energy needed
$Q_{charged}$	: The energy charged in the storage from the available energy
$Q_{discharged}$	: The energy discharged from the storage to provide load $Q_{difference}$
PCM	: Phase Change Material
NPV	: Net Present Value
Lf	: latent energy of phase change from solid to liquid

1. INTRODUCTION

1.1. Global Warming Scenarios

The historical utilization of worldwide natural resources has imposed a significant burden on the environment. This has resulted in environmental pollution, global warming, the exhaustion of our natural reserves, the jeopardy of biodiversity, and the elevation of sea levels. The current situation of climate change is an inevitable outcome of our past actions.

Burning fossil fuels like coal, oil, and gas for heat, electricity, and transportation is the main source of human-produced emissions. Each second, around 2.6 million pounds of carbon dioxide are released into the atmosphere—a number that continues to rise. Carbon dioxide levels have gradually increased from roughly 315 ppm (parts per million) in 1959 to an average of about 385 ppm in the atmosphere today. Current predictions indicate a further increase to as high as 500–1000 ppm by 2100. Figure 1.1 showcases changes in temperature and precipitation patterns (simulating a 4°C global warming by 2100) across seasons and annual means.

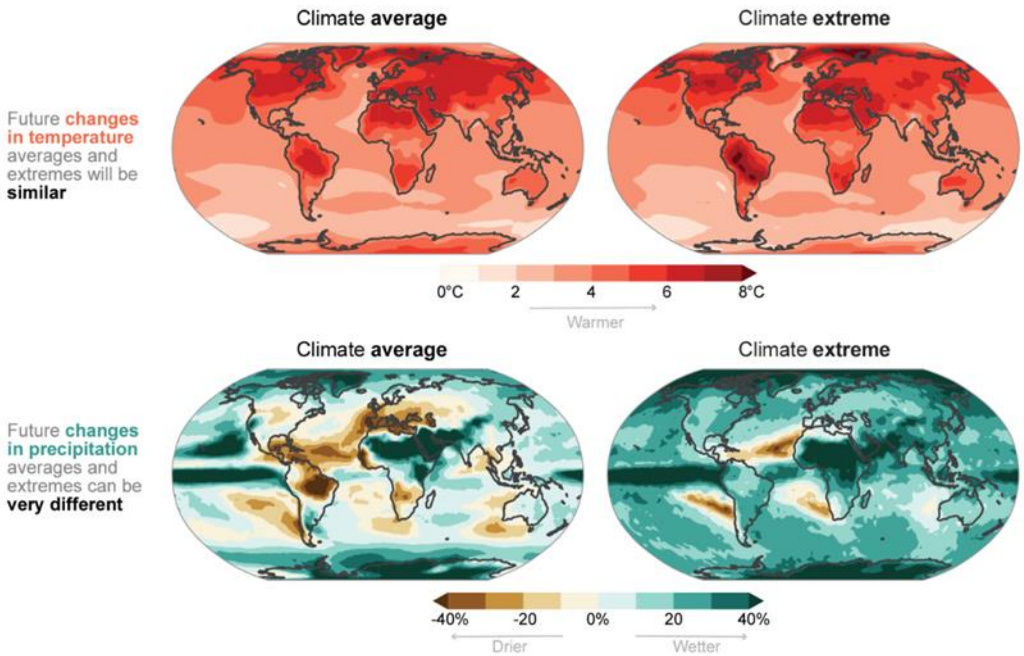

Figure 1.1. Spatial patterns of changes in the seasonal temperature and annual precipitation

As per the most recent report issued by the Intergovernmental Panel on Climate Change (IPCC), five distinct scenarios have been outlined, as depicted in Figure 1.2. These scenarios, referred to as shared socio-economic pathways, elucidate the outcomes of implementing swift and substantial measures, as well as the potential consequences in a scenario of no action being taken.

In the most unfavorable situation, the high-carbon trajectory, global temperatures could surge by over 4°C by the century's conclusion. To comprehend the gravity of this scenario, it's worth noting that it has been over 3 million years since the world encountered temperature escalations of greater than 2.5°C within such a short span.

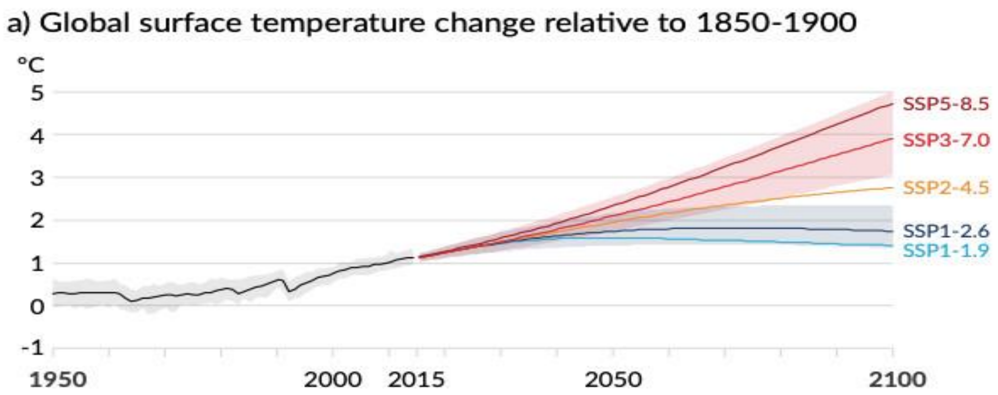

Figure 1.2. Global surface temperatures vary widely under different emissions pathways

It is well known that CO_2 is a greenhouse gas that captures solar radiation and contributes to global warming. According to scientists, doubling atmospheric CO_2 levels might lead to temperature increases of 2 to 4.5°C, caused by rapid changes such as snow and ice melt, and the behavior of clouds and water vapor.

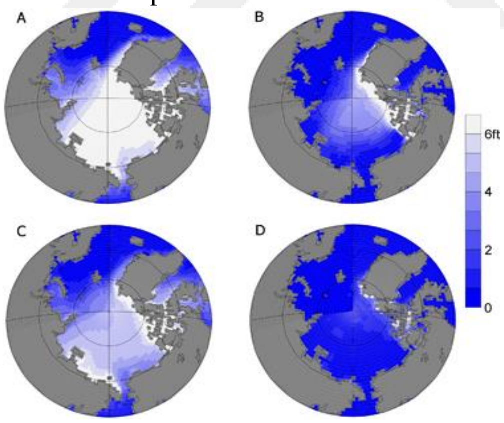

Figure 1.3. Sea ice thickness simulations

These maps shown in Figure 1.3 represent expected sea ice reduction. Sea ice thickness simulations from climate models for March and September, respectively, are shown in A and B. Sea ice thickness simulations from climate models are shown in C and D for March (C) and September (D) approaching the end of the twenty-first century. Future predictions show that March will have less ice (bluer in panel C), while September will have essentially no ice (almost all blue in panel D).

Once we exceed 2°C of warming (the internationally recognized "danger limit"), coastal flooding will impact millions. The consequences include reduced global food crop yields, extensive coral bleaching worsened by ocean acidification, heightened coral reef vulnerability, and an anticipated sea level increase of almost one meter by 2100. Additionally, the risk of extinction could loom over up to 30% of global species.

With temperatures rising by 3–4°C, a significant coral die-off will unfold (at this stage, corals are essentially doomed). Furthermore, as we persist on the trajectory toward the planet's sixth mass extinction, 40–70% of global species face the threat of being in jeopardy.

In South America and Central Asia, water supplies will be endangered due to glacier decline. There's also the concern that ocean hydrates and permafrost could release significant quantities of CO_2 and methane, potentially pushing global warming to an uncontrollable level. Additionally, if the Greenland and West Antarctic ice sheets were to disintegrate, leading to significantly more sea level elevation and inundation of coastal urban areas, a rise of at least one meter by 2100 and an eventual increase of 15 meters within the next 500 years could be expected.

As the temperature ascent persists, the potential for forest disappearance becomes more real. Trees play a crucial role in absorbing CO_2, thus if deforestation prevails and forest growth stalls, the environmental toll will be severe. According to the World Health Organization, the span from 2030 to 2050 could witness around 250,000 extra fatalities per annum due to the effects of climate change.

Envision a scenario where humanity not only remains inert regarding climate change but intensifies its negative impact, edging closer to critical thresholds beyond which irreparable damage is inevitable. The gravity of the situation lies in reaching a juncture where remedies become ineffective. In fact, the 2022 IPCC report emphasizes without ambiguity that human influence has been the unequivocal driver behind the warming of the atmosphere, oceans, and land. This declaration should serve as a striking alert, compelling us to enact essential transformations in our lifestyles—embracing practices like recycling and considering the adoption of green energy sources such as solar and wind power to fuel our residences

1.2. Türkiye’s Energy Policies

Among OECD nations, Türkiye boasts the most rapidly expanding energy market. Since 1990, Turkey has witnessed a staggering surge of 443.65% in its final electricity consumption and a noteworthy elevation of 374.13% in carbon dioxide (CO_2) emissions. The International Energy Agency (IEA) reveals that during the span of 2008 to 2018, Turkey experienced a robust 46.53% upswing in its total primary energy supply, with the total primary energy consumption concurrently escalating by 52.28%.

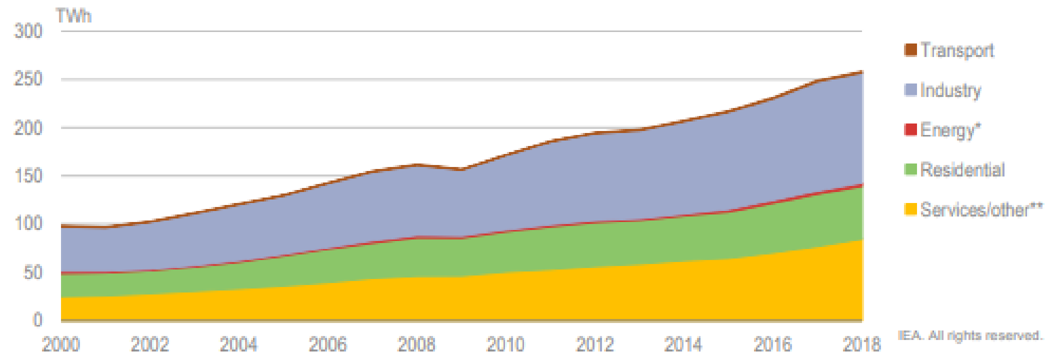

Figure 1.4. Electricity consumption by consuming sector, Türkiye, 2000-18

Türkiye's energy system heavily relies on fossil fuels, constituting 83% of total primary energy supply (TPES) in 2019 and 73% of total final consumption (TFC) in 2018 (Figure 1.4). Renewables, mainly geothermal and hydro, contribute the rest. Most oil and gas are imported, while about half of the coal and all renewable energy are produced domestically. Domestic energy production covered 31% of TPES in 2019. While traditional bioenergy for heating has declined, renewable energy production more than doubled since 2009, especially in geothermal, hydro, wind, and solar sectors. The industrial sector is the largest energy consumer (over a third of TFC in 2018), followed by transport (27%), residential (20%), and services (17%) (Figure 1.4).

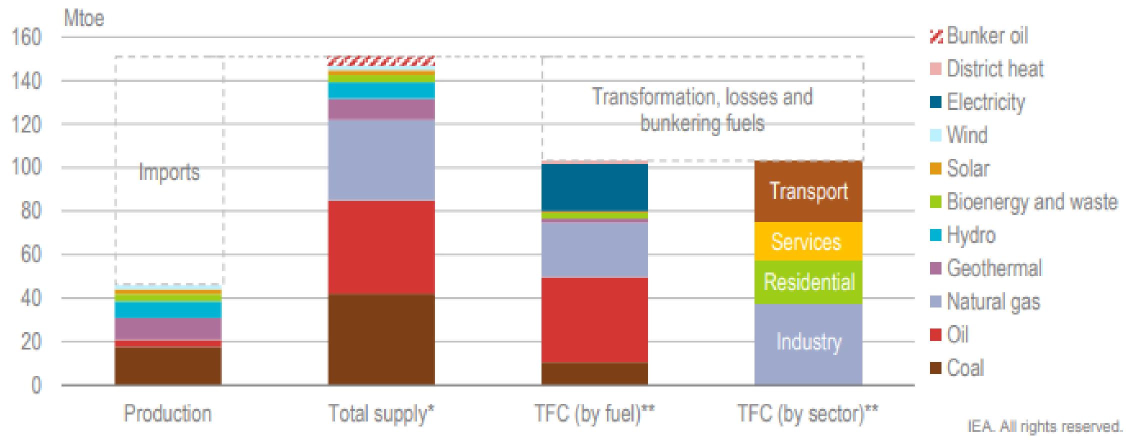

Figure 1.5. Overview of Türkiye's energy system by fuel and sector, 2018/19

Türkiye's current power system rests on four core components: production, where the state-owned company EÜAŞ (Elektrik Üretim Anonim Şirketi - The Electricity Generation Company) accounts for 15.9% of total electricity production. Transmission involves the high-voltage transmission network managed by TEİAŞ (Türkiye Elektrik İletim Anonim Şirketi - Turkish Electricity Transmission Corporation), responsible for transmitting electricity from power plants. Distribution encompasses the division of electricity distribution and sales responsibilities into distribution regions, managed by 21 private distribution companies. Lastly, the retail aspect handles end-user sales and services.

As indicated by the International Energy Agency's reports for 2019 and 2020, Türkiye's installed solar energy capacity, which stood at 5.6 GW by the close of 2020, is projected to surge to 15.1 GW with a twofold expansion by 2024. This extra 10 GW capacity will see a 3.7 GW increase from distributed energy systems. The same report outlines a substantial rise in renewable energy, with solar and wind energy spearheading the growth, and distributed systems contributing 530 GW out of the additional 1200 GW of installed capacity. As of August 2020, Türkiye's installed capacity has reached 93,022 MW according to data from the Ministry of Energy and Natural Resources. Within this, hydraulic energy holds 32%, followed by thermal power plants at 49.7%, wind, solar, and geothermal power plants at 8.6%, 6.8%, and 1.6% respectively, with other sources accounting for 1.3% (as depicted in Figure 1.5).

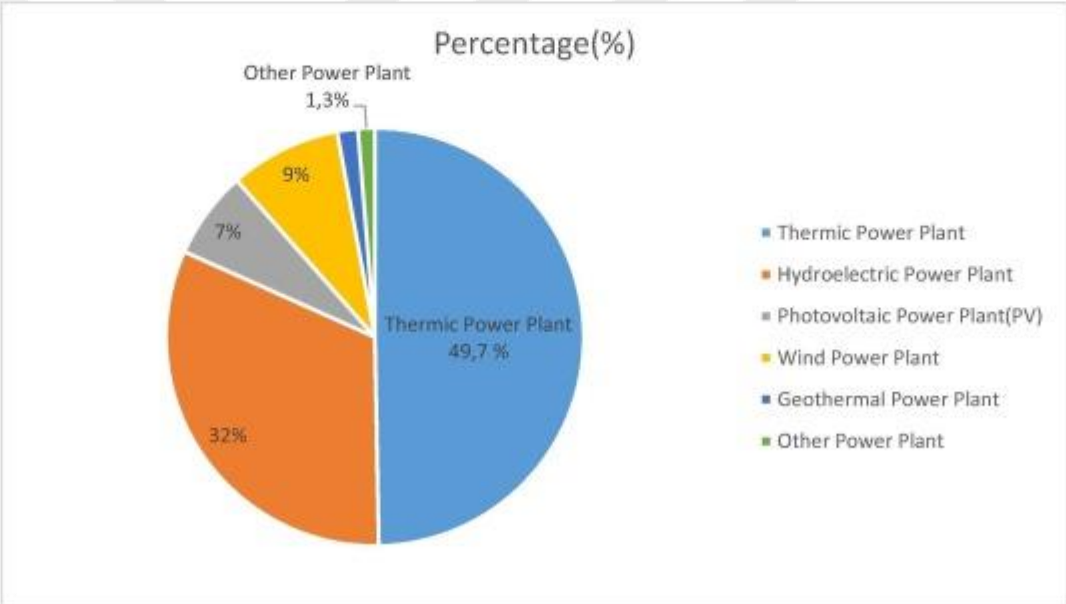

Figure 1.6. Türkiye's Percentage Installed Power According to Resource

Moreover, the count of power plants in Türkiye has reached 8934, encompassing those generating unlicensed energy. Within the operational power plants, there exist 669 hydroelectric, 68 coal, 262 wind, 52 geothermal, 330 natural gas, 6,435 solar, and 253 from other sources. Of these, 93% possess licenses, while the remaining 7% operate unlicensed. In terms of electricity usage, Türkiye recorded a consumption of 304.2 billion kWh and a generation of 304.8 billion kWh. Projections indicate a 4.8% surge in consumption up to 2023, reaching a total of 375.8 billion kWh..

Between 2006 and 2015, the average global temperature rose from 0.86 °C above the pre-industrial baseline to 1.04 °C above it. In response to this escalating global warming, the world has turned to renewable energy technologies. Thanks to both collective and individual efforts within the global community, investment in new renewables has been on the rise.

To attain its announced net-zero objective by 2053, Turkey is setting its sights on a minimum 35% reduction in emissions by 2030 compared to 2020 levels. Achieving this entails lowering emissions from 523.9 MtCO2e (million tons of carbon dioxide equivalent) in 2020 to 340 MtCO2e, aligning with the 2053 target. The Paris Agreement, ratified by 191 nations, seeks to curb the global temperature increase to 1.5°C to avert the climate crisis; Turkey joined as a party in October 2021. All participants at the previous year's summit pledged to enhance their emissions reduction objectives before COP27 in November 2022. To stay within the 1.5°C limit, global emissions must achieve net-zero status by 2050.

Hydropower once held undisputed dominance in renewable electricity generation in Turkey. It continues to lead as the largest source of renewable electricity, contributing to 29.2% of total electricity generation in 2019. Wind power takes the second spot, experiencing remarkable growth over the past decade thanks to the FiT system, surging from under 1.5 terawatt hours (TWh) in 2009 to 21.8 TWh in 2019. Wind power constituted 7.2% of total electricity generation in 2019. The rest of the renewable electricity stemmed from solar photovoltaics (PV) and geothermal energy, contributing 3.5% and 2.9% respectively to total electricity generation, while bioenergy accounted for 1.1% in 2019. Notably, geothermal and bioenergy for power generation nearly doubled within three years from 2016 to 2019.

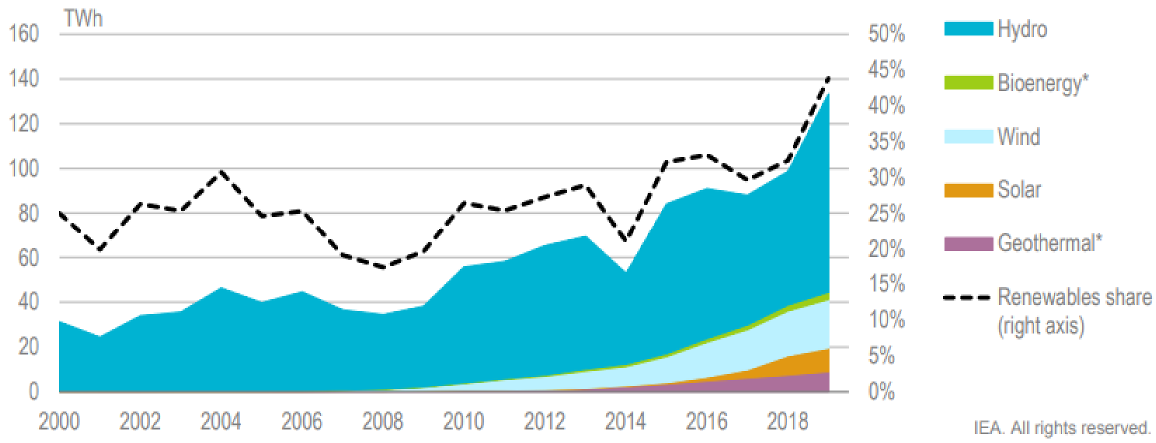

Figure 1.7. Renewable energy in electricity generation, Türkiye, 2000-19

Solar photovoltaic (PV) generation has displayed even swifter expansion, escalating from 3.7 TWh in 2017 to 10.6 TWh in 2018, marking a remarkable growth of 182% over two years. Collectively, renewable energy sources constituted 44% of total electricity generation in 2019. This positioning Türkiye towards the upper echelons in a comparison across IEA member nations.

Türkiye possesses substantial solar energy potential due to its geographic positioning. The average daily total radiation intensity reaches 4.18 kWh/m2/day, with an annual average of 1527.46 kWh m2/year. The yearly average sunshine duration extends to 2741 hours, with a daily average of 7.50 hours. As of 2020, Türkiye's installed solar power capacity stands at 6,294.7 MW, making up 6.8% of total production based on sources. Unlike the western and northern areas, the southern and eastern parts of the country receive more sunlight, a result of geographical factors. Notably, June and July exhibit the highest sunshine, while December and January record the least. This information is presented in the Solar Energy Potential Atlas (GEPA), visually depicted in Figure 1.8.

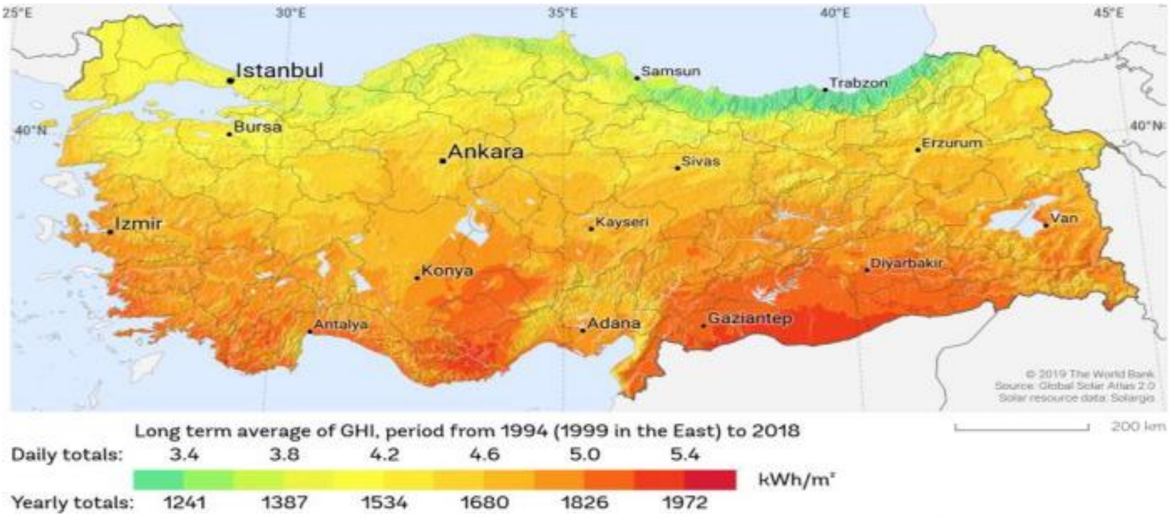

Figure 1.8. Türkiye's Solar Energy Potential Atlas

1.3. Literature Review

In regions with substantial solar irradiation potential, employing solar energy to operate air conditioning systems can prove advantageous, offering favorable outcomes in both technological aspects and economic considerations. Numerous researches have been conducted worldwide on systems used to transform solar energy into useful cooling. Two major methods of solar cooling are as follows: electrically driven methods utilizing PV and thermally driven methods utilizing collectors which include a variety of cooling cycles, like adsorption, desiccant, and absorption.

Most researches focus on thermal-driven solar cooling systems due to their high efficiency and reliability in large district cooling plants. Using the TRNSYS software, an assessment was conducted on the potential of an integrated solar absorption chiller ranging from 175 to 1400 kW, designed for cooling and heating in residential settings. This evaluation took place within the climatic conditions of Berlin (Germany), Lisbon (Portugal), and Rome (Italy). The numerical outcomes indicated that utilizing vacuum tube collectors instead of flat-plate collectors led to reduced economic feasibility, resulting in a decrease of solar collector area by

15–50%. It was determined that due to elevated maintenance and water consumption expenses, achieving a 60% annual solar contribution would only yield savings of 35% to 45% of operating costs (Mateus et al., 2009). An experimental configuration aimed to assess the functionality of a single-stage, 35 kW cooling capacity water lithium bromide (H2O–LiBr) absorption chiller was conducted. The chiller was energized by a flat-plate collector spanning 49.9 m2 in surface area, targeted for implementation in Spanish residences in Madrid during the summer of 2003. The system operated within heat rejection and generation temperatures ranging from 32–36 °C and 57–67 °C respectively. At peak insolation, the cooling effect generated was 5.13 kW, achieving a solar-to-cooling conversion efficiency of 11%. The utmost cooling capacity peaked at 7.5 kW, enabling an 8.67-hour duration of cooling provision. Throughout this span, the average, daily, and maximum Coefficient of Performance (COP) achieved were 0.34, 0.42, and 0.6 respectively (Syed et al., 2005). A study involving optimization analysis of collector area and cycle time was carried out for a 100 kW silica gel - water adsorption chiller in a single-stage, two-bed configuration. The chiller was driven by an evacuated tube solar collector and assessed under the climatic conditions of Bangalore. Employing TRNSYS V17 simulation, the research delved into the impact of varying operational parameters on the performance of the adsorption system. Results from the simulation indicated that the most favorable outcomes in terms of maximum Coefficient of Performance (COP) and solar fraction could be achieved with a collector tilting angle of 30° and an absorber area of 16 m2 (Jaiswal et al., 2016). A comprehensive exploration encompassing both experimental and numerical analyses was carried out on a groundbreaking high-temperature solar cooling system. This innovative system centered around flat-plate evacuated solar thermal collectors (SC). Notably, the system integrated a double-effect 21 kW absorption chiller, distinguishing it as the inaugural solar cooling system founded on non-concentrating solar thermal collectors. Experimental findings revealed a collector peak efficiency surpassing 60%, while the daily average efficiency hovered around 40%. In addition, from an economic perspective, outcomes demonstrated that the novel prototype displayed commendable profitability, as evidenced in the study (Buonomano et al., 2016).

However, most of the existing residences especially in cities, cannot be equipped with central large cooling plants. Therefore, there is a great tendency towards electrically driven small cooling systems using PV Panels. A study in a hot summer zone in Beijing, China, analyzed a quasi-grid-connected photovoltaic-powered DC air conditioner. The investigation examined the technology's working principle and showed that it can reduce grid electricity usage by more than 67% and 77% during summer daytime and nighttime, respectively. The solar-powered air conditioner exhibited an overall energy efficiency ratio 4.6 times higher than that of a standard air conditioner (Liu et al., 2017). A performance study of a grid-connected photovoltaic-powered central air conditioner was conducted in the South China climate, involving practical operation for an office building. The study employed three indices—solar fraction (SF), net solar fraction (NSF), and surplus energy ratio (SER)—to evaluate the system's effectiveness. The research revealed that meteorological conditions notably impacted the system's performance, with SF varying based on prevailing weather patterns. Furthermore, NSF and SER exhibited significant trends linked to these patterns. Notably, SF was particularly high in April, September, and October due to reduced cooling loads. The annual average values for SF, NSF, and SER were found to be 51.62%, 104.5%, and 52.72%, respectively (Li et al., 2018). A study conducted a techno-economic analysis of a hybrid solar PV-grid powered air-conditioner designed for daytime office use in hot humid climates, specifically focusing on Kumasi city, Ghana. The case study revolved around a standard 30 m2 office space. The experiment employed a pure sine wave hybrid inverter equipped with an integrated PWM charge control system. The findings indicated that, for a nominal cooling capacity of 2.5 kW and maximum power consumption around 1.19 kW, a 1040 Wp solar PV system with a 200 Ah, 24 V battery configuration achieved a monthly mean solar fraction of 51% ± 9%. The system was projected to generate approximately 1211 kWh of energy per year. From a financial standpoint, the analysis unveiled potential savings of US$1600 compared to 100% utility grid electricity, and about US$3300 savings could be realized when the air-conditioner operates on 100% solar energy as opposed to 100% utility grid electricity over a 10-year period (Opoku et al., 2018). An experimental analysis was conducted on an air conditioner that operated on photovoltaic energy while also being supplemented by grid power. The study utilized a 3.52 kW cooling capacity air-conditioner designed for a 35 m2 floor area. In Alicante, Spain, a photovoltaic setup with three 235 Wp panels directly connected to the equipment at 24 Vdc was employed. The findings indicated that the system achieved energy efficiency ratings (EER) and solar fractions (SF) reaching close to 15% and 65% respectively. These outcomes were observed over a 6-month monitoring period (Aguilar et al., 2017). The viability of a solar electric-vapor compression refrigeration (SE-VCR) system aimed at cooling applications in the southern area of Turkey was assessed. The Cooling Load Hourly Analysis Program (HAP) 4.4 was employed to compute the hourly fluctuations in the system's parameters. The findings indicated that the system could adequately fulfill the compressor's power requirements through a photovoltaic panel surface area spanning 31.26 m2, and with a peak compressor power consumption of 2.53 kW (Bilgili et al., 2011).

One of the most interesting HVAC systems is the variable refrigerant flow VRF. These systems are energy efficient and provide considerable comfort to occupants. (Amarnath et al., 2009) conducted a study where they installed a VRF system in nine offices located in Knoxville. This installation aimed to offer separate heating and cooling to each office. The outcomes of the study indicated that the occupants showed a preference for the VRF system in comparison to the pre-existing ducted space conditioning system. Moreover, when delivering a specific cooling level at the same external temperature, the VRF system showcased a reduction in energy consumption by 20-40%, concurrently enhancing the comfort of the occupants. To assess the economic viability of both constant refrigerant flow (CRF) and variable refrigerant flow (VRF) systems for an office building in Qatar operating for 12 and 24 hours a day, researchers presented a life-cycle cost analysis. The outcomes of this analysis demonstrated that, considering the entire lifespan, the VRF system exhibited a lower present-worth cost compared to the CRF system. This cost reduction was attributed to the VRF system's lower operating costs (Atalla et al., 2022). Utilizing the Energy Plus environment, a novel VRF module was created, and an assessment was made by contrasting the energy usage of the VRF system with both a variable air volume (VAV) system and a fan-coil plus fresh air system (FPFA). The findings of the study revealed that the VRF system offers the potential for energy savings of approximately 22% when compared to the VAV system, and about 11% when compared to the FPFA system (Zhou et al., 2007). A comparative analysis was undertaken to assess the effectiveness of the Variable Refrigerant Flow (VRF) system when compared to the Roof Top Unit (RTU) variable-air-volume (VAV) system. This study was conducted at a test building situated in Oak Ridge, Tennessee, USA. The outcomes of the field test indicated that the VRF system achieved a reduction of about 17% in energy consumption during cooling operation and roughly 74% during heating operation, in comparison to the RTU system. Additionally, the VRF system's energy consumption was lower by approximately 55% compared to that of the RTU system (Lee et al., 2018). An examination was carried out regarding the energy efficiency and power generation capabilities of a variable refrigerant flow (VRF) heat pump system integrated with photovoltaic (PV) technology within a 5-story residential building in Cyprus. The findings revealed that the VRF system's annual power consumption ranged from 14,005 to 18,710 kWh. In parallel, a PV array boasting a total capacity of 13 kW was able to generate an annual output ranging between 23,200 and 23,650 kWh. This translated to the PV arrays satisfying approximately 126-166% of the building's annual VRF energy demand. The integration of the PV system also led to a reduction of around 14 tons of CO_2 emissions each year. Additionally, the economic feasibility evaluation indicated that the project's net present value could vary from $4,843 to $13,355 over a 20-year investment duration (Gilani et al., 2021).

One of the primary difficulties encountered in solar cooling is aligning the energy generated with the energy consumed, a task that heavily relies on the effectiveness of energy storage solutions. Moreover, a notable gap exists in research pertaining to photovoltaic (PV) air conditioning modules tailored for off-grid functionality. In solar photovoltaic refrigeration systems, the inclusion of batteries becomes imperative. Presently, despite advancements in the operational features of different system components, lead-acid batteries remain the sole viable choice for electrical energy storage. In their study conducted in South Africa, (Gayapershad et al., 2021) explored the sizing, selection, and cost assessment of a fully off-grid photovoltaic DC-powered air conditioning (AC) system. This system integration included a charge controller, an inverter, and deep cycle batteries. The cooling load for the specified area was determined to be nearly 1 ton, resulting in the selection of a package-type vapor compression system. For its operation, 6x 335 watts solar panels were chosen and connected in series.The analysis outcomes indicated that, depending on the required operational duration, either 2 x 48 V DC, 150 Ah batteries or 6 x 48 V DC, 150 Ah batteries were needed to supply backup power for 8-hour or 24-hour operation, respectively. Additionally, the coefficient of performance (CoP) for the system was determined to be 2.7. Moreover, the cost analysis revealed that the final system was projected to cost approximately $6,829 (USD) for 24-hour operation and a complete off-grid setup. A study involving experimental research on photovoltaic air conditioning systems utilizing the direct drive approach was presented. This study set up an off-grid system configuration at the Al-taje site in Iraq during the summer season. The system components comprised an array of eight photovoltaic panels, a 75Ah battery bank for power storage, a PWM (pulse width modulation) charge controller, and a DC air cooler. The experimental outcomes demonstrated the effectiveness of this DC air conditioning system in coping with Iraq's warm climate. It served as a viable alternative to conventional air conditioning systems (AC air conditioners), which tend to consume substantial amounts of electrical energy. The implemented system provided a fully operational room cooling solution powered entirely by solar energy (Hussein et al., 2020). Through simulations and optimization analysis, an assessment was carried out to determine the economic viability of a building in Iraq. This involved conducting a comparative study to evaluate the economic feasibility of employing a PV electrical grid for a cooling load of 600 kW, as well as a standalone solar PV system. The outcomes of numerical analysis indicated that the utilization of a PV system could result in an approximate 45% reduction in electrical power consumption compared to reliance on grid power (Mohammed et al., 2022). An investigation was carried out on an efficient off-grid solar-powered DC air conditioning system. The study involved suggesting a solution aimed at enhancing the energy efficiency of conventional air conditioning systems. This enhancement was achieved by replacing the standard alternative current motor (AC) with a direct current brushless motor (BLDCM), which would be powered by photovoltaic (PV) panels. The main objective was to decrease energy consumption and subsequently lower the electricity expenses associated with cooling and refrigeration in off-grid regions, specifically within KSA. The results of the study indicated that the proposed technique effectively reduced energy consumption to less than half of what is consumed by AC air conditioners (Khlifi et al., 2021).

The utilization of a thermal storage tank presents an appealing technology, facilitating the transfer of thermal energy from periods of surplus to periods of demand. Moreover, innovative designs aimed at enhancing energy efficiency were explored. In their study (Hoseini Rahdar et al., 2016), the analysis of a vapor compression AC system was conducted using two hybrid strategies. Initially, an ice thermal energy storage (ITES) system was employed, followed by the use of a phase change material (PCM) tank to establish a comprehensive storage mechanism capable of shifting the load from on-peak to off-peak periods. The outcomes of the study revealed that the payback period for the PCM system, in comparison to the conventional system, was approximately 5.56 years, while for the ITES system, it was 3.16 years. Furthermore, the power consumption of the ITES and PCM systems exhibited reductions of 4.59% and 7.58% respectively, compared to the conventional system. Additionally, CO_2 emissions produced by the ITES and PCM systems were found to be 17.8% and 27.2% lower respectively, in comparison to the emissions generated by conventional systems.

The effectiveness and performance of cold thermal energy storage systems for off-grid PV air-conditioned buildings remain uncertain. To address this, a feasibility and performance assessment was conducted, comparing various storage features. The study incorporated a feasibility analysis and employed cost optimization to determine optimal configurations for residences, offices, and hotels. Results showed significant cost reductions in the residential scenario: 49.76% for chilled-water storage, 41.77% for ice storage, 44.31% for phase change material (PCM) storage, and 22.78% for building thermal storage (Hu et al., 2022). A novel residential PV air-conditioning system, employing a compression chiller, was introduced. This system integrated ice storage with low-temperature phase change materials (PCMS). The research design involved utilizing ice storage to fulfill typical cooling requirements, while the low-temperature PCMS was strategically designed to address freezing demands. Through a comprehensive system-energy analysis involving various parameters such as PV areas, storage capacities, and insulation thicknesses, it was demonstrated that the new system could achieve energy savings of up to 85%. Notably, this system displayed higher cost-effectiveness compared to a battery-only system under specific electricity price scenarios (Beck et al., 2015). A study focused on improving grid connection through a solar-electric driven heating and cooling system with phase change material (PCM) storage. The study involved coupling a solar-electric driven variable refrigerant flow (VRF) 3-pipe system with a 20 kWh thermal storage capacity using PCM Parafol 16-97 for crystallization. Simulations were conducted for Photovoltaic-Arrays with a 30° inclination, and the results showed a latent heat storage capacity of 16 kWh. The system incorporated a heat exchanger comprising six units, each with a length of 23 m, enabling storage at peak power levels exceeding 10 kW during charging. Notably, the study demonstrated that the PCM storage component significantly improved system efficiency during discharge, leading to an increase in the Energy Efficiency Ratio (EER) from 5 to nearly 6. This enhancement helped lower electrical demand and reduce grid stress (Shex et al., 2017).

1.4. Motivation

Many of the papers presented in the literature review above focus on integrating the combination of the solar PV system with DX-type units which requires high energy consumption. VRF systems are worldwide increasing in residential as well as in business buildings. Due to easy installation and easy access to energy, source/heat sink, air/air-based systems are getting more and more relevant. Thus, integrating the VRF system will reduce energy losses and thus enhances the overall efficiency of the system.

In addition, most researches study the integration of PV panels with batteries in order to provide the cooling needs for different apartments. This system will lead to a very high payback period due to the expensive costs of replacing these batteries. Whereas few studies conducted on PV-driven VRF systems, the capability to store energy is limited in these systems. Systems with electric batteries are expensive and sensible thermal storage does not fit well into the refrigeration cycle due to energetic losses. The ability to store energy is mandatory to achieve better integration of PV-production for such combined systems. Thus, a new strategy for energy storage using phase change materials for cooling systems is needed to be investigated.

Furthermore, most of these systems described in these researches were not sized to provide all the energy needed year through without using any auxiliary non-renewable source. Their proposed design was based on a maximum solar fraction of around 80%. Thus, an auxiliary conventional system is still needed to meet this fluctuation between supply and demand.

Based on all of the above-mentioned points, and in the wake of increasing focus on sustainability and the 'go green' movement, the idea flourished investigating the performance of a PV solar-electric driven variable refrigerant volume VRF system for an apartment in Adana, Türkiye, and studying its validity, reliability, and feasibility. This system can provide the cooling loads of this apartment. And cold thermal storage based on phase change material is used to enable the stability and the continuous run of the system without the use of any non-renewable auxiliary energy source. Thus, enhancing the feasibility of the system by removing the expensive battery storage.

1.5. State of Art - "PV-Driven VRF System Using Cold Thermal Storage"

The present paper will investigate the performance of a solar electrical-driven VRF system combined with a cold phase change material storage. A residential villa in Adana, Türkiye will be taken as a case study. A thermo-economic optimization methodology will be adopted in order to find the suitable capacities of the different components. Then a feasibility study will be conducted in comparison with the conventional PV-Batteries system. The paper will follow the following outline:

- Conventional Building Model: starting from finding the hourly site information data. Then based on Türkiye Thermal Standard the Conventional Building Model will be created.
- Optimized Building Model: using energy conservation and thermal efficiency measures (for example enhancing the building thermal envelope, economizer mode etc), the Optimized Building Model will be created.
- System Mathematical Model for the different components PV, VRF, PCM, and Battery will be provided.
- Thermo-economic Optimization Sizing Methodology to provide a 100% solar fraction for the two systems:
    - Conventional PV-Battery-VRF
    - PV-PCM-VRF
- Simulation Results comparison between these two systems.
- Feasibility Study comparison with respect to the baseline scenario of the two systems.

2. BUILDING MODEL

2.1. Adana Site Information Data

In order to evaluate the benefits of the proposed model, a local baseline villa in Adana, Türkiye was taken as a case study. Türkiye is witnessing a great increase in electrical consumption. In fact, it has the fastest-growing energy market within OECD countries. Based on statistical agencies buildings are responsible for one-fourth of the energy consumption. Since space heating and cooling has a major part in this consumption, climate conditions play a prominent role. Based on the Turkish Contractors Association, space cooling accounts for the space-based energy requirement which is nearly 30% of the consumed energy.

The Koppen Climate Classification subtype for Adana (37°N, 35.25°E) climate is "Csa"(Mediterranean Climate). Based on Koppen the average temperature for the year in Adana is 18.9°C. The coolest month on average is January, with an average temperature of 9.4°C, and the lowest recorded temperature of -7.8°C. The warmest month, on average, is August with an average temperature of 27.8°C, and the highest recorded temperature of 42.2°C.

Map data		Per year	
Direct normal irradiation	DNI	1824.4	kWh/m²
Global horizontal irradiation	GHI	1770.7	kWh/m²
Diffuse horizontal irradiation	DIF	652.8	kWh/m²
Global tilted irradiation at optimum angle	GTI opta	2029.2	kWh/m²
Optimum tilt of PV modules	OPTA	32 / 180	°
Air temperature	TEMP	18.9	°C
Terrain elevation	ELE	125	m

Map

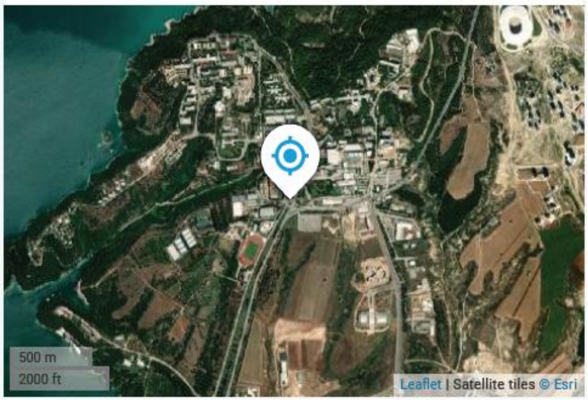

Figure 2.1. Global Solar Atlas Adana Site Info

Türkiye, in terms of its solar energy potential winner due to its geographical location between $36^{o}$and 42^{o} latitudes has a big solar energy potential and an opportunity to benefit from this endless energy source in building design, developing renewable energy technologies, agriculture, and many other applications compared to many other countries. For January, the monthly average of daily total radiation is 1.23 kW h m^{-2} day^{-1}, while for July, it is 6.55 kW h m^{-2} day^{-1}. The annual average value of daily total radiation is 3.81 kW h m^{-2} day^{-1}.

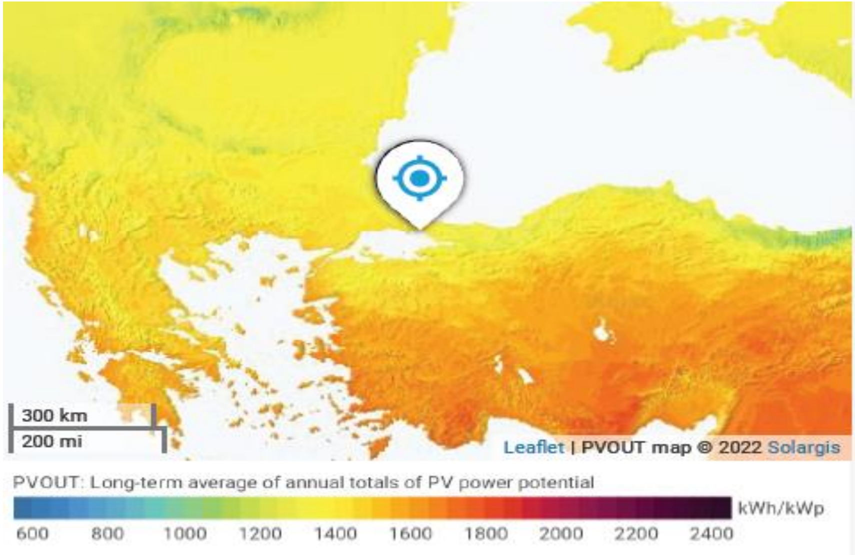

Figure 2.2. Global Solar Atlas PVOUT

Studying the sun-paths as showing Figure 2.3 provides information on the length of the day and the amount of daylight received throughout the year, which are important insights for assessing the solar system's performance since the irradiation on a tilted surface depends mostly on the Sun's position. The worst-case scenario, when the solar system produces the least amount of energy, is December because the sun's path is lower in the winter than it is in the summer.

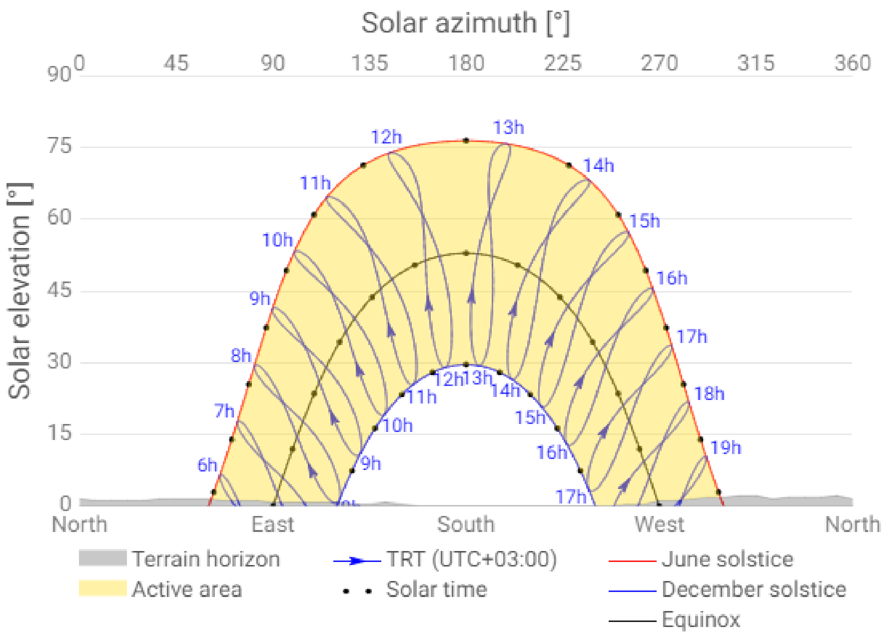

Figure 2.3. Horizon and sun-path for Adana

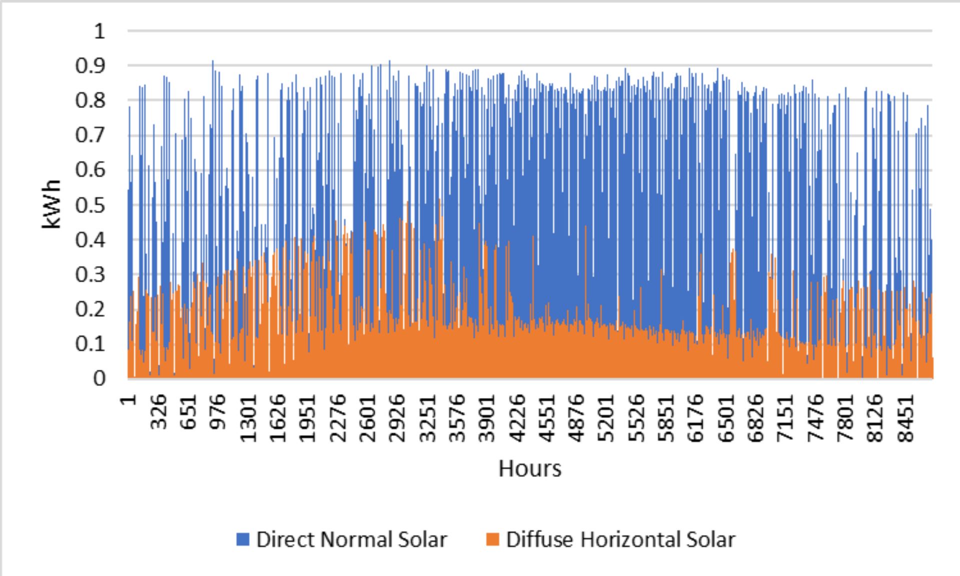

Figure 2.4. Adana's hourly direct normal and diffuse horizontal solar irradiances

The hourly direct and diffuse solar irradiances illustrated in Figure 2.4 for Adana show the amount of hourly solar radiation that reaches the villa over 1 year. The graph displays two lines: one for the direct solar irradiance and one for the diffuse solar irradiance. The direct solar irradiance line represents the amount of solar radiation that is received directly from the sun. This radiation is not scattered or diffused, and it is typically the strongest during the middle of the day when the sun is highest in the sky. The diffuse solar irradiance line represents the amount of solar radiation that is scattered or reflected by the atmosphere before reaching the earth's surface. This radiation is less intense than direct radiation and is usually more evenly distributed throughout the day. Overall, the graph provides important information about the amount of solar radiation that is available in Adana at different times of the day. This information is useful for understanding the potential for solar energy production.

2.2. Baseline Building Model

The residential villa was designed in accordance with the regionally adopted local style of architecture, as seen in Figure 13. The villa is a two-story residence with a total surface of 300 m2 and a total volume of 1425 m3, A family of ten members could fit there comfortably. A 3D model of the villa was created using the "Design Builder" simulation program to simulate the building's behavior under actual operating conditions.

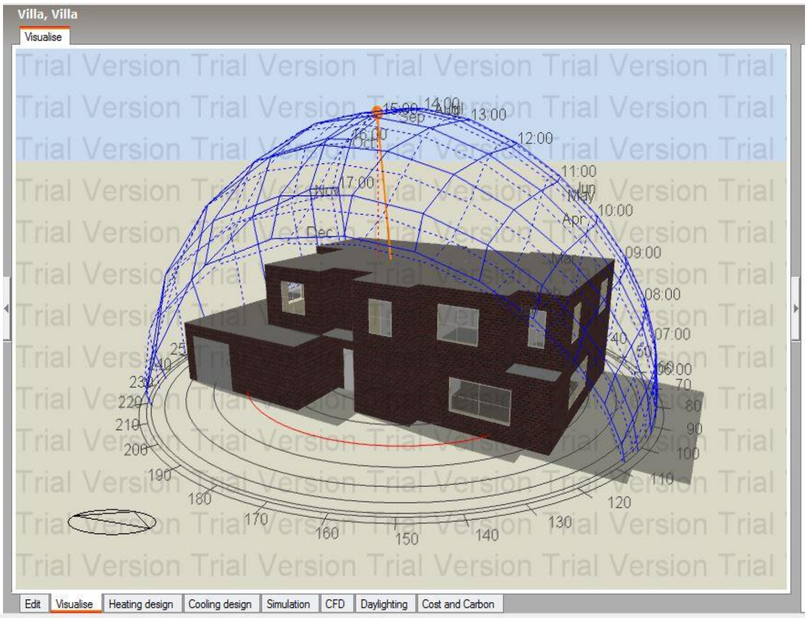

Figure 2.5. Villa's Model

The fresh air requirements, external infiltration, occupancies, lighting, and appliances associated with their schedules for each room are based on the ASHRAE standards 90.2 and 62.1 as shown in Table 2.1.

Table 2.1. General Comfort and Gains Properties

Comfort and Gains					
Indoor set point temperature	^{o}C	22	Internal gains (peak)	kW	3
Indoor Relative humidity	%	50	Average/Maximum Occupancy	Nr.	5/10
Infiltration	Vol/h	0.3	Solar Heat Gain Coefficient	%/100	0.25
Lighting (peak)	W/m^2	20	Visible Transmittance	%/100	0.25

In addition, according to TS 825 Thermal Insulation Requirements in Buildings in Türkiye as for Adana is considered in the first region. Table 2.2 shows how the thermal transmittance characteristics of the walls, roofs, and glazing are determined using Türkiye Thermal standard values.

Following the import of all of these values into the simulation program, the "Design Builder" will evaluate all of the thermal gains from external ventilation, heat transmission through the building envelope, glazing, shading effect, and radiation for the multi-zones. The model is simulated based on the real hourly ambient weather conditions obtained from the International Weather for Energy Calculations (IWEC)

In other words, this project was applied to Adana's Case Study. In order to proceed, the Villa’s Thermal Characteristics and activities were implemented on Design Builder so that we can extract the thermal balance and the required hourly cooling load. Moreover, the hourly solar irradiance and weather data of the area were also reported. Finally, one more input should be considered: the roof area of the Villa. Determining the area will allow us to have an idea about the number of PVs that could be installed on the roof.

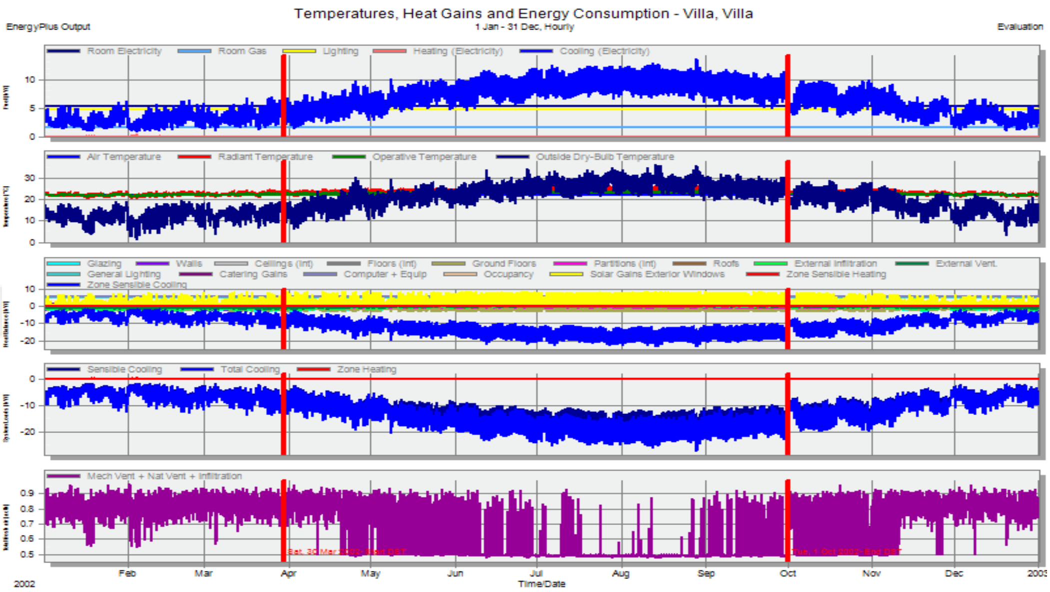

Figure 2.6. Baseline energy consumption output

Therefor the baseline model is a model designed according to the TS 825 Turkish Thermal Insulation Requirements in Buildings used to calculate the cooling load of the villa using the "Design Builder" simulation program. This program is used to simulate the energy performance of a building, considering the climate and building characteristics of the area, as well as the insulation and other construction materials used. It considers the ventilation, solar gain, and infiltration of the building, and then calculates the resulting cooling load.

The TS 825 requirements in Buildings dictate the thermal characteristics of the building materials, as well as the overall thermal performance of the building, in order to ensure that it meets the standards set for energy efficiency. By using this simulation program and the TS 825 requirements, the baseline model is used to determine the cooling load of a building and to ensure that it meets the necessary energy efficiency requirements. Variations of the hourly cooling load for different months are shown in Figure 2.6, the cooling load results in Design Builder appeared in negative signs because the simulation software is calculating the energy that is leaving the space. Heat energy leaving space is considered a negative load, while heat energy entering the space is considered a positive load.

The sensible cooling load of a Variable Refrigerant Flow (VRF) system is not static but instead is constantly changing throughout the day in response to the outside temperature. This is due to the system's variable-capacity nature, which is capable of adjusting its cooling output in relation to the building's cooling demand. As the outside dry-bulb temperature rises, the sensible load and cooling electric demand of the VRF system increases accordingly. This is a great benefit of VRF systems compared to other conventional cooling systems, as it allows for more efficient temperature regulation.

2.3. Optimized Building Model

Energy losses are one of the major factors in the design of the energy process. To account for these losses, the majority of thermal systems are built with capacities that are much higher than necessary. Therefore, energy conservation and efficiency measures have been implemented in order to prevent overdesigning and demonstrate its importance. These actions will lower peak load capacities as well as annual energy consumption. The "Design Builders" simulation program has been used to perform a parametric study to determine the best thermo-economic value for each variable parameter. The thermal transmittance values of the walls, roofs, and glazing are among these parameters. Table 2.2 lists the various parameters used in local thermal building (LBV) and those used in the optimized building model (OPV).

Table 2.2. Thermal Transmittance Values

Thermal Characteristics	Units	Type	Adana
Wall Thermal Transmittance	$W/(m^2.K)$	LBV	0.7
		OPV	0.4
Roof Thermal Transmittance	$W/(m^2.K)$	LBV	0.45
		OPV	0.3
Window Thermal Transmittance	$W/(m^2.K)$	LBV	2.4
		OPV	1.6

In order to reduce the heat gains from direct solar radiation, exterior shading on windows has also been taken into consideration. In the main rooms, occupancy sensors have also could be installed. If the room is not occupied, these sensors will raise the indoor temperature to the predetermined setback value. As shown in Figure 2.8, an inclined double roof (tilted angle = 37 degrees) has been added which will provide shading and a free area to handle the solar panels. Finally Increasing the setpoint temperature for cooling by 1 degree from 22 ^oC to 23 ^oC can lead to potential energy savings in annual consumption. Raising the setpoint temperature reduces the cooling load and may result in shorter or lower-capacity operation of the cooling system, thereby reducing energy usage. While occupant comfort and regional climate should be considered, a 1 ^oC adjustment is generally within the acceptable comfort range. Although the immediate savings seem small, cumulative effects over time can lead to significant energy reductions and cost savings.

Table 2.3. Thermal Reduction Percentage from LBV

Thermal Parameter	Units	Adana	
		CL	ACE
Walls U-Value	%	2%	1%
Roof U-Value	%	1%	2%
Glazing U-Value	%	6%	1%
Setback Temperature	%	3%	5%
Overall OPV	%	12%	9%

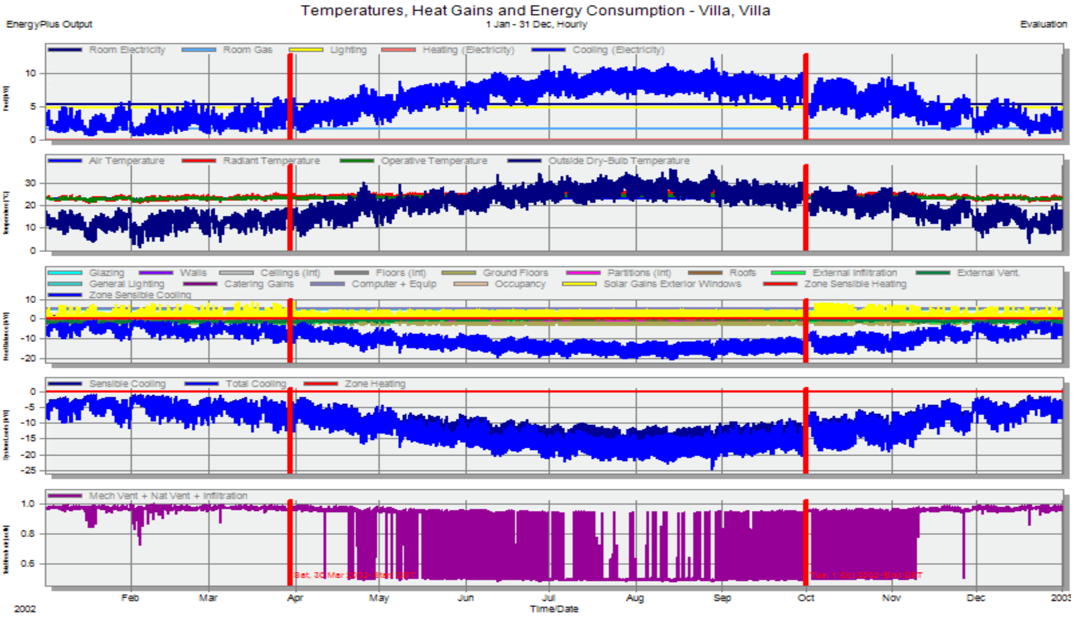

Figure 2.7. Optimized model energy consumption output

The overall and individual parametric reduction percentages in the cooling load (CL) and annual cooling energy (ACE) required are summarized in Table 3. The results demonstrate that using the optimal values (OPV) will reduce the cooling load needs by 12%, and the annual cooling energy needs by 9% if compared to the baseline characteristics (LBV) in Adana.

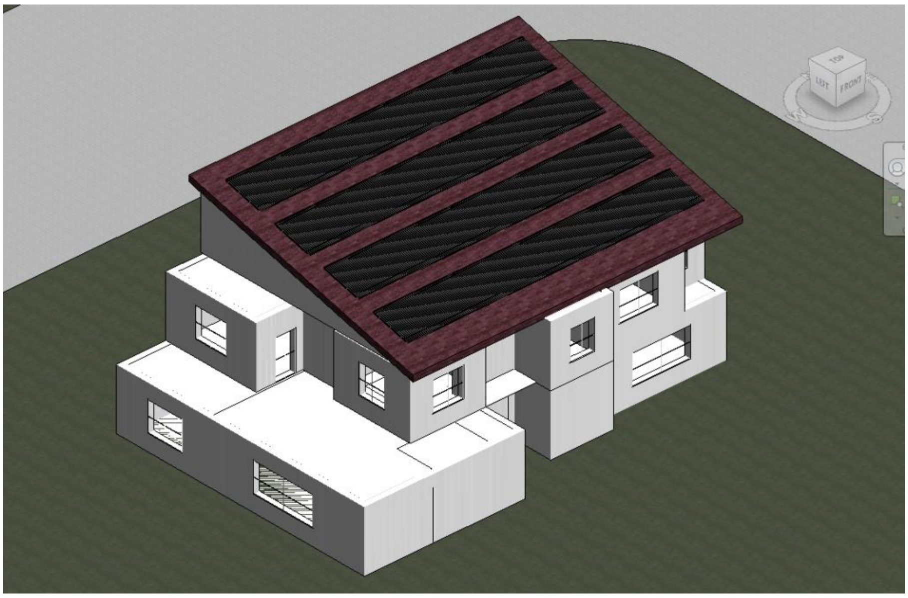

Figure 2.8. OPV Architecture

3. MATHEMATICAL MODELS

3.1. Solar Irradiance on PVs

Solar irradiance is the amount of solar energy that reaches a given area in a given time. It is the most important factor in determining how much power a solar photovoltaic (PV) system can generate. PV systems require direct sunlight for optimal operation and performance. Therefore, the amount of solar irradiance on a PV system has a direct impact on its electrical output. Direct radiation is the solar energy that comes directly from the sun and is unaffected by the atmosphere. This is the most efficient type of solar energy due to the lack of atmospheric interference. Diffuse radiation comes from the sun’s reflection off clouds, dust, water vapor, and aerosols. This type of radiation is less efficient than direct radiation because the atmosphere has scattered and absorbed some of the energy. The amount of diffuse radiation varies throughout the day, depending on weather conditions. The direct and diffuse radiations on the solar collector must be calculated based on the equations provided, taking into consideration the tilt angle (β) of the solar collector and its orientation (south-facing). The total global radiation (G) on the tilted Solar Collector Panels is:

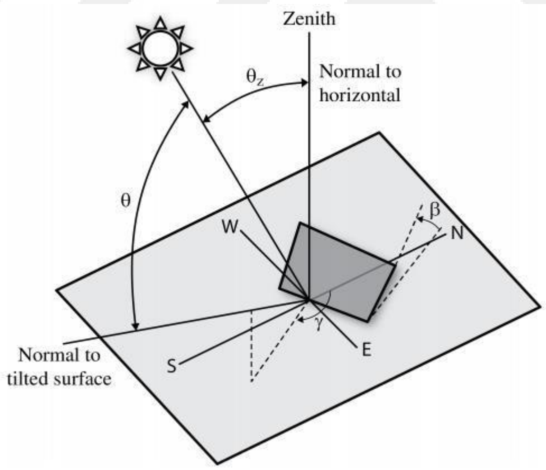

Figure 3.1. Solar Angles for the Tilted Panels

$$G = G_d + G_{diff} \tag{3.1}$$

$$G = G_{dn}.\cos(\theta_i) + G_{diff\_H}.\frac{1+\cos(\beta)}{2} \tag{3.2}$$

where:

G_d: is the corrected direct incident solar radiation on the tilted solar collector(KW/m^2)

G_{dn} : is the direct normal incident solar radiation given from site information(KW/m^2)

G_{diff} : is the corrected diffuse incident solar radiation on the tilted solar collector**(**KW/m^2)

G_{diff_H}: is the diffuse horizontal incident solar radiation given from site information (KW/m^2)
θ_i: Angle of incidence of the radiation beam with respect to the normal to the tilted plane, which can be calculated from the following equation:

$$\cos(\theta_i) = \cos(\theta_z) . \cos(\beta) + \sin(\theta_z) . \sin(\beta) . \cos(A - \gamma) \tag{3.3}$$

θ_z: Zenith angle between the vertical and the line of the sun given from site information
β : Tilt angle of the panels
γ : Azimuth of the normal to the tilted plane equals 0 since the plane is directed toward the south
A: Azimuth horizontal angle measured clockwise from the South (> 0 westward)

3.2. Variable Refrigerant Flow Unit

Then the hourly energy rate PPV that could be produced by the number of panels (first variable: N) of the PV was calculated. The method of modeling the performance of the PV panel includes mathematical equations to calculate the current, voltage, and power generated at the specified temperature and irradiance, by considering that the PV system includes a maximum power point tracking (MPPT) system. Thus, PPV could be calculated as follows:

$$P_{PV} = G \times A_p \times N_p \times \eta_p \tag{3.4}$$

Where P_{PV} is the electrical hourly energy rate which could be produced based on the available hourly solar irradiances. A_p is the area of one panel. N_p is the total number of panels. η_p is the efficiency of PV panels which includes the effect of temperature, irradiances, and MPPT controller.
The resulting out cooling power will be:

$$\dot{Q}_{cooling,available} = P_{PV} * COP \tag{3.5}$$

Where $\dot{Q}_{cooling,available}$ is the cooling energy hourly rate which could be produced from the VRF unit whenever the electrical energy hourly rate is available from the PV panels.

3.3. PV System

The utilization of photovoltaic (PV) systems is gaining popularity worldwide, with their applications continuously evolving and adjusting. Most of today's PV systems are compact, connected to the grid, and capable of generating a few kilowatts of power. Nevertheless, advancements like Maximum Power Point Tracking (MPPT) and enhanced system implementation have brought about transformations in the utilization and applications of PV technology. Photovoltaic systems utilize the fundamental principles of a conventional p-n junction diode to convert solar energy into electricity. This involves the absorption of photons at the junction, leading to the conversion of absorbed energy into the material's electron system. This process generates separated charge carriers, which can manifest as either electron-ion pairs within a liquid electrolyte or electron-hole pairs within a solid semiconductor. These charge carriers induce a potential gradient in the junction region, subsequently gaining acceleration in the presence of an electric field. This acceleration enables their movement as an electrical current through an external circuit. The electric power converted into electricity can be calculated as the square of the current multiplied by the resistance of the circuit.

A common technique employed in modeling a PV array is to determine the current and voltage generated at a given temperature and irradiance using mathematical equations based on the power output at Standard Temperature Conditions (STC), which is defined as a radiant energy of 1000 W/m2, an air temperature of 25° C, and an incidence angle of 48.2°. This calculation takes into account the associated factors and analyzes how they influence the energy produced.

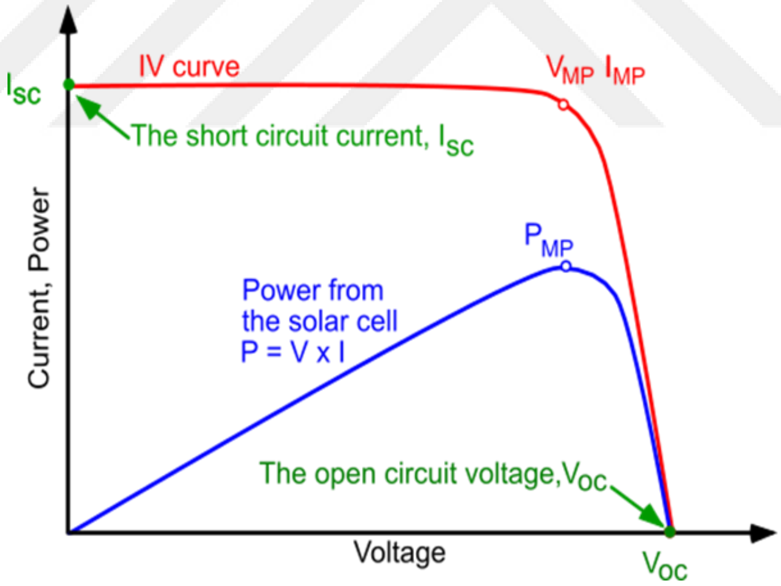

Figure 3.2. PV Current / Voltage Characteristic

When modeling photovoltaic systems, the distinct voltage-current curve of the PV panel (as seen in Figure 3.2) must be taken into consideration. The PV current-voltage (IV) curve is a graph that shows the relationship between the current and voltage of a photovoltaic (PV) cell under varying levels of illumination. It can be used to determine the efficiency of a particular PV cell or module, as well as its output characteristics under different lighting conditions. The IV curve typically has a curved shape, with the current increasing as the voltage increases. The shape of the curve is affected by the type of material used in the cell, as well as the number of cells in the module. Three key points are used to determine the model's parameters: the short circuit current (Isc) when there is no voltage, the Maximum Power Point (MPP) - when the panel produces the most power, at this point, the current is IMPP and the voltage is VMPP.

The third point corresponds to the open circuit voltage, where the current reaches zero and the voltage reaches the open circuit voltage value. These specific voltage and current values are distinct for each PV array and are specified in the manufacturer's datasheet.

The use of electrical equivalent circuits is one method for modeling PV arrays. One of the most common equivalent circuits is the single-diode model, in which the PV cell is represented by a circuit consisting of a single diode and two resistors, as illustrated in Figure 3.3.

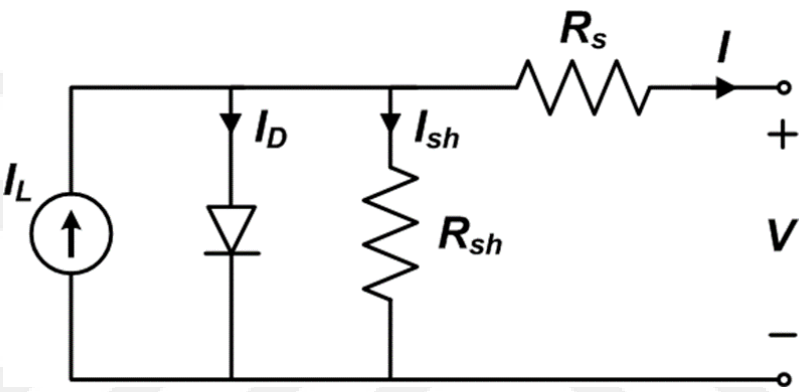

Figure 3.3. Circuit Model of PV panel

Illustrated in Figure 3.3, the PV cell is depicted as a configuration consisting of a current source in tandem with a parallel diode, as well as a parallel resistor (Rsh) and a series resistor (Rs) connected to the current source. The direct current source IL embodies the current resulting from the interaction between photons and electrons within the PV cell. The diode within the model captures the p-n junction phenomenon, symbolizing the non-linear behavior of the PV cell. This diode allows current to flow when the cell is illuminated. Conversely, the parallel resistance Rsh mirrors current losses, and the series resistance Rs represents voltage losses attributed to the cell's metallic contacts. Hence, the characteristic equation governing this circuit is delineated as follows:

$$I_{pv} = I_L - I_D - I_{sh} \tag{3.6}$$

This equation can be written in the following form:

$$I_{pv} = I_l - I_0 \left(e^{\frac{V+I.R_{sh}}{A}} - 1 \right) - \frac{V + I.R_s}{R_p} \tag{3.7}$$

where:

$$A = \frac{mKT}{q} \tag{3.8}$$

K is the Boltzmann constant (1.38 × 10-23 J/K), q is the elementary charge (1.6 × 10-19 C), T corresponds to the solar cell temperature, m is the correction coefficient ranges between 1 and 2, and $I0$ is the internal p-n junction saturation current.

The alternative approach to model a PV array involves the utilization of mathematical formulas to compute the current, voltage, and irradiance produced under given temperature and irradiance conditions. This is achieved by extrapolating from the power generated at Standard Temperature Conditions (STC), where one assesses the various influencing factors and their impact on power generation. STC, denoting Standard Temperature Conditions, corresponds to specific parameters including an irradiance of 1000W/m2, a temperature of 25 °C, and an air mass of 1.5.

If the PV system does not include a maximum power point tracking (MPPT) system, the current supplied by the panels during hour t is calculated as follows:

$$I_{pv}(t) = I_{SC}.\frac{G(t)}{G_{STC}} \tag{3.9}$$

where:

I_{sc} : PV generator short-circuit current in (A)

$G(t)$: average irradiance over the surface of the PV panels during hour t (W/m^2)

G_{stc} : irradiance at STC, which is equal to 1000 W/m^2.

To be more precise, we must consider the effect of temperature on the PV. The PV cell temperature

T_C [°C] can be calculated using:

$$T_c(t) = T_a(t) + \left(\frac{NOCT - 20}{800}\right).G(t) \tag{3.10}$$

where:

T_a is the ambient temperature [℃]

NOCT is the nominal operation cell temperature [℃] (typically 45 ℃)

As a result, the output current must be corrected in the following manner:

$$I_{pv}(t) = I_{SC}.\frac{G(t)}{G_{STC}}.\left[1 + \frac{\mu_{I,OC}}{100}.(T_C(t) - 25)\right] \tag{3.11}$$

where:

$\mu_{I,OC}$: temperature coefficient of I_{SC} [%/°C].

Whereas if the charge controller includes an MPPT system, the PV panels will always operate at the maximum power point of the current curve, resulting in a higher output current from the PV.

$$I_{pv}(t) = I_{mp}.\frac{G(t)}{G_{STC}}.\left[1 + \frac{\mu_{I,OC}}{100}.(T_C(t) - 25)\right] \tag{3.12}$$

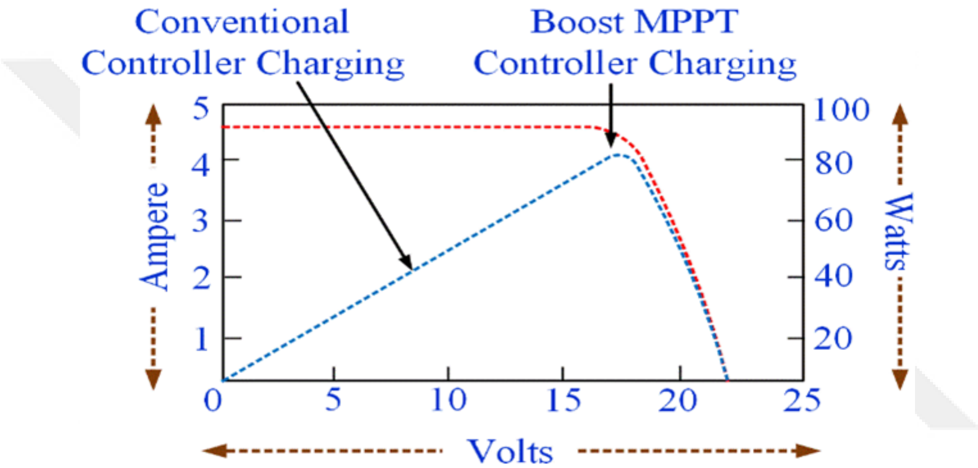

Figure 3.4 PV characteristic using MPPT controller

$$V_{pv}(t) = V_{pm}.\frac{G(t)}{G_{STC}}.\left[1 + \frac{\mu_{V,OC}}{100}.(T_C(t) - 25)\right] \tag{3.13}$$

where:

Imp and Vmp are the operating current and voltage at maximum power point and is given in the datasheet of the PV panel.

Therefore, the resulting power will be:

$$p_{pv}(t) = V_{pv}(t).I_{pv}(t) \tag{3.14}$$

3.4. Lead Acids Batteries

Batteries hold a paramount role in the evaluation of renewable energy system investments. Consequently, effectively managing these systems to maximize battery longevity stands as a foremost concern. This objective can be accomplished through the regulation of battery charging and discharging cycles. Accordingly, it is imperative to appropriately size the system, ensuring a continuous supply to meet the load demand while concurrently minimizing the overall system costs. The utilization of battery modeling and simulation within the context of hybrid system design, as currently under investigation, serves a dual purpose. Firstly, it facilitates an examination of the battery's performance as an independent energy storage unit. Secondly, it empowers the optimization of battery dimensions and lifespan to curtail operational expenses.

When engaging in battery modeling, consideration of multiple intricate factors becomes imperative, rendering this stage notably intricate. Among these factors are State of Charge (SOC), voltage levels, internal resistances, capacitance, charge resistance, discharge resistance, and various other non-static variables. Even in the present era, lead-acid batteries maintain their position as the most widely utilized battery type for power applications. While they present diverse energy densities, their efficiency excels particularly in lower power density scenarios. Despite their high energy density capabilities, the scope of power density they offer remains limited. This limitation has implications for the amount of energy accessible within the system and the duration required for battery charging.

Due to lead acid batteries having a fairly short lifespan, they must be routinely replaced. This is the main obstacle for isolated power generation. It is crucial to take into account that renewable energy sources are volatile, and the power supplied is largely determined by the weather. Consequently, an assessment of all the system components must be done prior to installment to make sure the load is supplied with the needed power at all times. The battery's capacity to store and deliver energy is therefore essential to ensure a standalone system can handle the load. This will help to prevent any deficiencies and rectify them before they arise. The battery is charged by the solar generator, which stores the energy and can provide it in the necessary amount and at the necessary time. Batteries charged with photovoltaic energy can be used to power many devices in remote and risky areas. Photovoltaic systems offer a steady supply of electricity regardless of the weather or time of day, as they are capable of storing electrical energy. It is essential to properly manage the system to extend the life of the battery, including controlling its charging and discharging cycles. Additionally, the system should be adequately sized to guarantee the load is met by the supply while decreasing the overall cost of the system.

The battery storage was considered initially to be full, then it enters in discharging and charging phases as per the energy difference rate between the electric energy rate needed for the VRF and its corresponding available electric energy rate from the solar PV-VRF combination in an hourly basis.

$$\dot{Q}_{diff,e} = P_{PV} - \dot{Q}_{electric,needed} \tag{3.15}$$

Discharging Mode If the needed cooling electric energy rate at a specific hour is greater than the available electric energy ($\dot{Q}_{diff,e} < 0$). The energy deficit will be extracted from the battery's storage. And the discharged energy rate can be calculated as follows:

$$\dot{Q}_{discharged,e} = \frac{\dot{Q}_{diff,e}}{\eta_{storage,e}} \tag{3.16}$$

Charging Mode: If the available electric energy rate at a specific hour is greater than the needed electric cooling energy load, the excess cooling energy will be stored in the batteries storage. In this case, the charging energy rate will be as follows:

$$\dot{Q}_{charged,e} = \dot{Q}_{diff,e} \times \eta_{storage,e} \tag{3.17}$$

The Thevenin model of lead acid batteries is a mathematical model used to represent the behavior of a lead acid battery when it is connected to a load. The model illustrated in Figure 3.5 is composed of a voltage source, an internal resistance and an external resistance connected in series. The voltage source represents the potential difference between the positive and negative terminals of the battery and can be used to calculate the amount of power that the battery can deliver to the load. The internal resistance represents the effect of the internal chemical reactions of the battery on the current flow. The external resistance represents any external resistance that the load may generate, such as the resistance of the wires connecting the battery to the load.

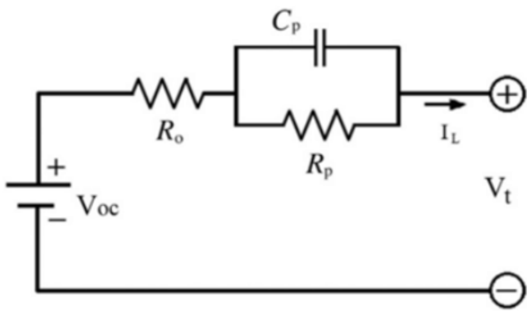

Figure 3.5. Thevenin Circuit

In the initial parallel branch, there exists a resistor symbolizing the battery's resistance to over-voltage. Meanwhile, the second parallel branch encompasses a capacitor symbolizing the capacitance existing between the electrolyte and the electrodes. As none of these factors possess dynamic attributes, the dynamic accuracy of this model is inherently limited. This is due to the omission of the battery's state of charge from the considerations. This configuration proves advantageous for applications that do not necessitate the incorporation of dynamic state of charge considerations.

The discharging phase of lead acid batteries involves the flow of energy from the battery, typically as electrical power. During discharge, the lead acid battery consumes active material from the positive plates and transfers it to the negative plates. This process produces electrical current and lowers the battery's state of charge. The duration of the discharging process depends on the rate of discharge, the capacity of the battery, and the depth of discharge. When the battery is almost fully discharged, the voltage begins to decrease, signaling the need to recharge the battery.

The discharging equation is given by the following equation:

$$V = [2.085 - 0.12(1 - \mathrm{SOC})] - \frac{1}{C_{10}}\left(\frac{4}{1 + I^{1.3}} + \frac{0.27}{SOC^{1.5}} + 0.02\right)(1 - 0.007\Delta \mathrm{T}) \quad (3.18)$$

The initial component represents the alteration in open circuit voltage caused by the state of charge, reflecting changes in electrolyte concentration. Meanwhile, the second component arises from fluctuations in internal resistance, amalgamated as the summation of all series resistances.

The Temperature Difference is given by the following formula considering that the reference temperature is 25 °C

$$\Delta T = T - 25 \quad (3.19)$$

In addition, the State of charge will be defined by the equation:

$$SOC = 1 - \frac{Q}{C} \quad (3.20)$$

where:

Q (I.t) is the charge delivered at the time of interest

C is the battery’s capacity

The discharge process is regarded as having 100% efficiency. Nevertheless, the quantity of usable charge available during discharge is constrained by the current rate and temperature in alignment with the capacity. This ultimate value is normalized concerning the discharge current associated with the C10-rated capacity (I10), and the expression is as follows:

$$\frac{C}{C_{10}} = \frac{1.67}{1 + 0.67(I/I_{10})}(1 + 0.005\Delta T) \tag{3.21}$$

When the discharge current approaches zero, the greatest capacity that may be removed is approximately 67% more than the C10 capacity at 25°C. The Charging equation is given by the following equation:

$$V = [2 - 0.16\text{SOC}] - \frac{1}{C_{10}}\left(\frac{6}{1 + I^{0.86}} + \frac{0.48}{(1 - SOC)^{1.2}} + 0.36\right)(1 - 0.025\Delta\text{T}) \tag{3.22}$$

In this case, the state of charge (SOC) is a function of the efficiency conversion C and SOC0. The SOC equation is given as:

$$SOC = SOC_0 - \frac{\eta_c Q}{C} \tag{3.23}$$

And the Efficiency equation will be:

$$\eta_c = \mathbf{1} - exp\left[\frac{20.73}{\frac{I}{I_{10}} + 0.55}(SOC - 1)\right] \tag{3.24}$$

3.5. Cold Phase Change Material Thermal Storage

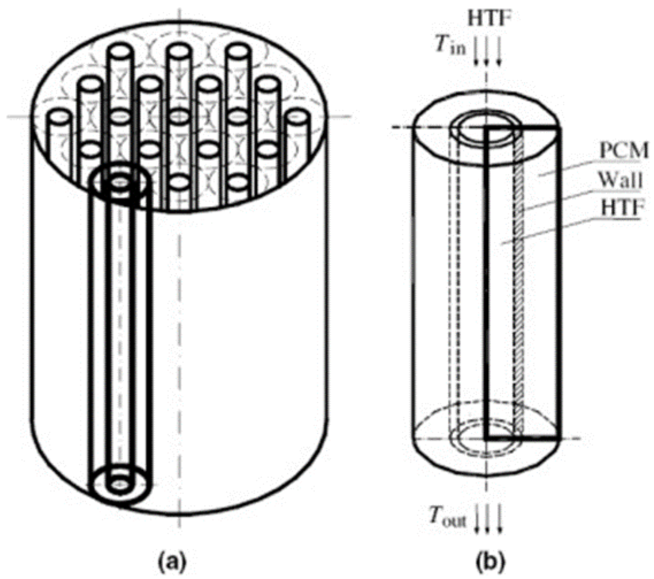

Figure 3.6. PCM Storage

The PCM thermal storage tank was designed to bridge the divide between the chilled water thermal energy rate and the amount of energy the VRF can produce. This tank uses phase change material (PCM) as the energy medium, which has the ability to absorb and release heat energy. When in charging mode, the VRF produces more energy than the chilled water thermal energy rate demands, and this excess energy is stored in the PCM tank. This stored energy can then be used when the chilled water thermal energy rate is higher than the amount of energy the VRF can produce. The PCM tank allows for the storage of this excess energy for later use, reducing the need for additional energy sources and helping to improve energy efficiency.

The maximum amount of energy that can be stored in the CPCM storage is calculated using the following Equation:

$$Q_{CPCM} = \rho_{CPCM} \times V_{CPCM} \times \lambda \tag{3.25}$$

where:
ρ_{CPCM}: Density of the CPCM material
V_{CPCM} : PCM storage volume
λ : Latent energy of phase change from solid to liquid.

The PCM system will be designed so that when solar energy is available and the cooling load needed is fulfilled, the cooling load will be provided directly from the solar system and any energy excess will be stored in the PCM system. However, when the cooling load is higher than the solar electrical power, the PCM will be used in order to close the gap and this power will be $\dot{Q}_{difference}$. The storage was considered initially to be full, then it enters in discharging and charging phases as per the energy difference rate between the cooling energy rate needed and its corresponding available energy rate from the solar PV-VRF combination on an hourly basis.

$$\dot{Q}_{difference} = \dot{Q}_{cooling,available} - \dot{Q}_{cooling,needed} \tag{3.26}$$

Where $\dot{Q}_{cooling,needed}$ is the cooling hourly energy rate calculated from the building energy model simulation performed in the “Design Builder”.

It was assumed that initially, the storage is full, then it enters in discharging and charging phases as follows:

As seen in Figure 3.7, Initially the liquid fraction of melt f = 1, then the maximum enthalpy of PCM:

$$H_{\max} = \rho_l * \lambda \tag{3.27}$$

$$V = \frac{Q_{\max.stored}}{H_{\max}} \tag{3.28}$$

where:

$H_{\max}$= is the maximum enthalpy at the end of the phase change $f = 1$ in kWh/m^3

ρ_l = is the liquid density PCM in Kg/m^3

λ = latent heat of fusion in kWh/Kg

$Q_{\max.stored}$ = maximum storage needed in kWh

V = Storage volume in m^3

Discharging Mode If the needed cooling energy rate at specific hour is greater than the available cooling energy ($Q_{difference} < 0$). The deficit in energy will be extracted from the PCM storage tank. And the discharged energy rate can be calculated as follows:

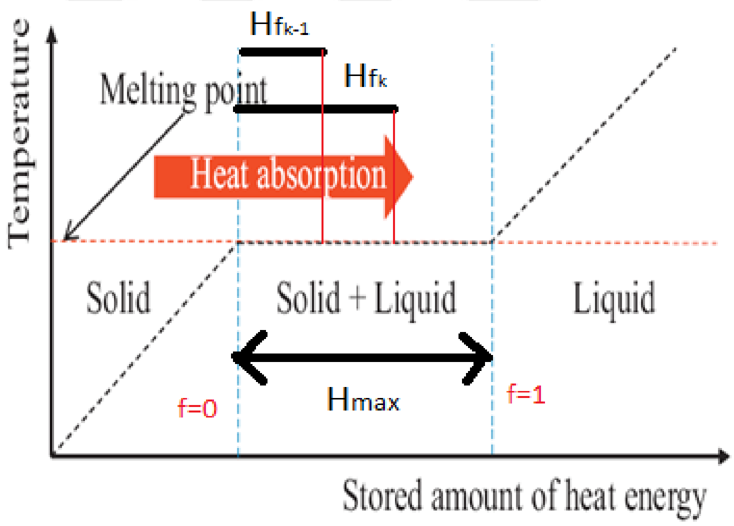

Figure 3.7. PCM Storage during Discharging Phase

$$\dot{Q}_{discharged} = \frac{\dot{Q}_{difference}}{\eta_{storage}} \tag{3.29}$$

The energy level inside the PCM will decrease until it reaches a minimum value when $f_k = 0$.

$$V * H_{f_k} = V * H_{f_{k-1}} - \left|\dot{Q}_{discharged}\right| \tag{3.31}$$

$$H_{f_k} = \rho_l * f_k * \lambda \tag{3.30}$$

where:

$Q_{discharged}$ = is the energy discharged from the storage to provide load $Q_{difference}$ in KWh.

$\eta_{storage}$ = efficiency of PCM storage

H_{f_k} = PCM enthalpy (KWh/m^3) at melt fraction $f = f_k$; and k is the number of hours from starting discharging.

$H_{f_{k-1}}$ = PCM enthalpy (KWh/m^3) at melt fraction $f = f_{k-1}$; and k-1 is the number of hours from starting discharging

A limitation of that $H_{f_k} > 0$ so that the melt fraction $f \neq 0$ and the PCM will not be in a solid

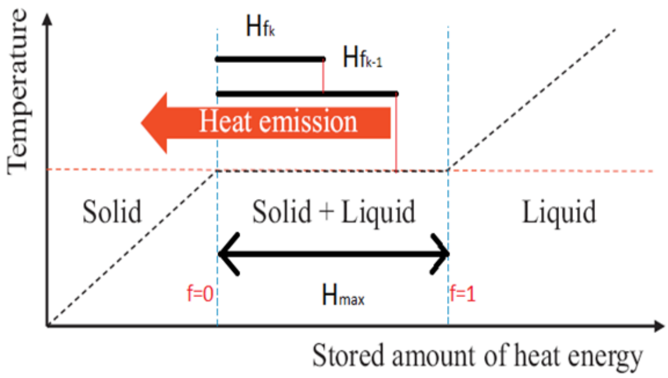

state. If $H_{f_k} = 0$ the storage is empty, and an auxiliary heat source is needed:

$$Q_{aux} = Q_{cooling,needed} - (Q_{cooling,available} + Q_{storage}) \tag{3.32}$$

Charging Mode: If the available cooling energy rate at a specific hour is greater than the needed cooling energy load ($\dot{Q}_{difference} > 0$), the excess cooling energy will be stored in the PCM buffer

Figure 3.8. PCM Storage during Charging Phase

storage tank. In this case, the charging energy rate will be as follows:

$$\dot{Q}_{charged} = \dot{Q}_{difference} \times \eta_{storage}$$

()

The energy level inside the PCM will increase until it reaches a maximum value when $f_k = 1$.

$$V * H_{f_k} = V * H_{f_{k-1}} + \left|\dot{Q}_{charged}\right| \tag{3.33}$$

$$H_{f_k} = \rho_l * f_k * \lambda \tag{3.34}$$

where:

$\dot{Q}_{charged}$ is the energy that could possibly be charged in the storage from the available energy

$Q_{difference}$ until the storage reached its maximum load ($V * H_{\max}$).

A limitation of that $H_{f_k} \leq H_{\max}$ so that the melt fraction $f \leq 1$ and the PCM will not be in a liquid state totally.

4. SYSTEMS CONFIGURATION AND OPERATION

4.1. PV-Batteries-VRF

Solar energy is becoming an increasingly popular way to power cooling systems, such as Variable Refrigerant Flow (VRF) systems. A VRF system is an energy-efficient and cost-effective cooling system that consists of an outdoor heat pump, refrigerant lines, and indoor fan coil units. Photovoltaic (PV) panels are installed on the roof and connected to the VRF unit. These panels generate energy from solar irradiances (sun's rays), which are then used to power the VRF unit. Any excess energy generated from the PV panels can be stored in batteries storage through an inverter for times when solar energy is not available. These batteries provide the necessary power to the VRF unit when solar energy is not available, primarily at night. The cooling energy supplied by the VRF unit is then directed to the building's fan coil units through refrigerant pipes. This provides the building with the necessary cooling demand without relying on traditional power sources, such as electricity from the grid. Solar energy is an effective and efficient way to power cooling systems, as it is cost-effective and reduces the building's reliance on traditional energy sources.

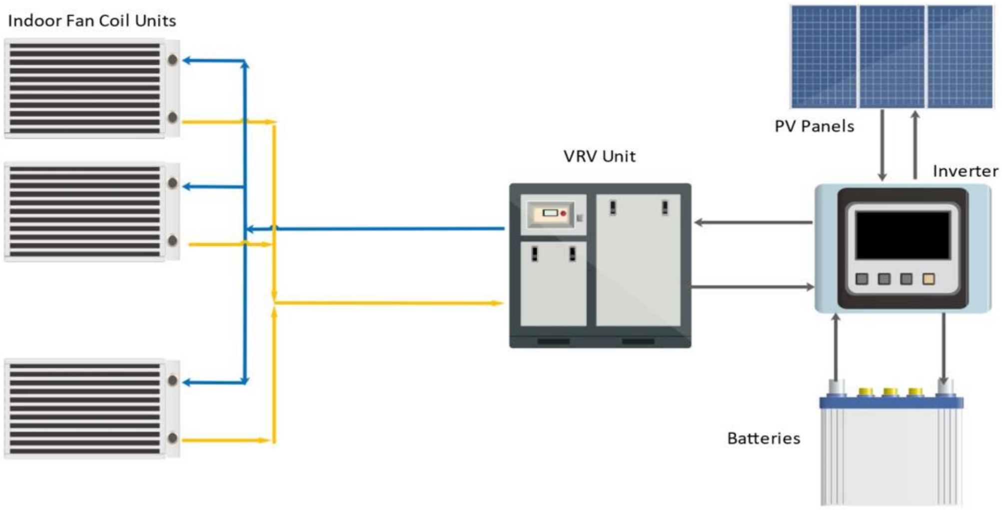

Figure 4.1. VRF Batteries system components integration

Figure 4.1 shows the different components of the conventional system. It consists of: Photovoltaic panels, variable Refrigerant Flow Unit, batteries, inverter and indoor Fan Coil Units.

4.2. PV-PCM-VRF

Our proposed system aims to replace traditional electric storage methods with latent thermal storage. This is done by utilizing Variable Refrigerant Flow (VRF) technology to convert solar energy into cooling energy. This energy is then stored in a cold phase change material buffer tank through refrigerant pipes that use its high latent solid-liquid phase change energy to store a huge amount of energy in a small volume. A chilled water pump is then used to circulate the chilled water through pipes to the fan coil units, providing the necessary cooling energy. This process enables buildings to reduce their energy consumption while relying on renewable energy sources. The direct use of solar energy to provide cooling has the benefit of avoiding the need for costly and inefficient energy storage batteries. The latent thermal storage provided by the phase change material buffer tank is much more efficient than traditional electric storage methods, allowing for more efficient and cost-effective cooling of buildings.

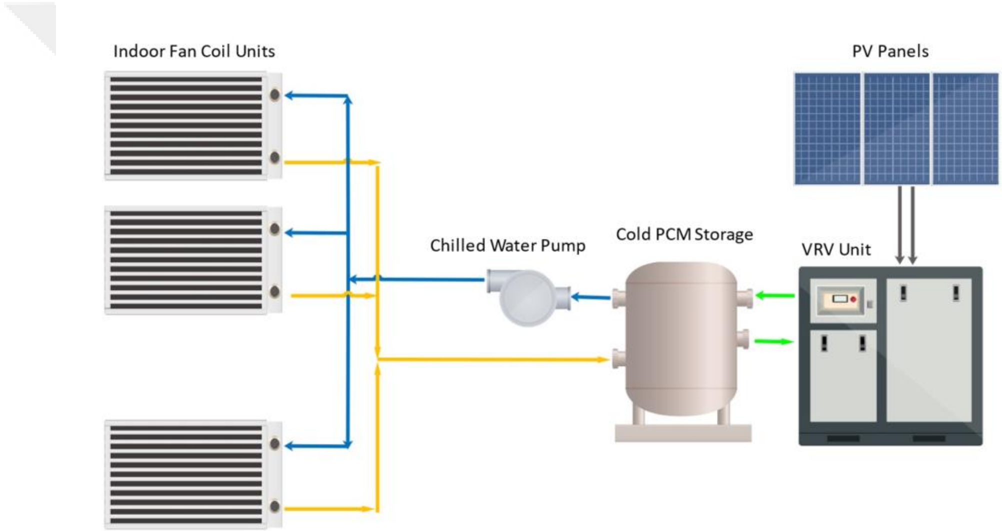

Figure 4.2. VRF PCM system components integration

Figure 4.2 shows the different components of the proposed system. It consists of:

1- Photovoltaic panels.
2- Variable Refrigerant Flow Unit.
3- Phase Change Material cold storage
4- Chilled Water Circulating Pump
5- Indoor Fan Coil Units

5. COMPONENTS SELECTION AND SPECIFICATIONS

5.1. PV Panels

The off-grid solar system captures sunlight to store energy in a battery bank for structures beyond the main power grid. Solar panels convert sunlight into DC electricity, which flows through a solar charge controller ensuring proper, non-excessive charging. This controller helps "float" the battery bank, maintaining optimal charge. The current is then directed to the battery for storage. In off-grid solar setups, power is drawn from the battery through a DC-to-AC solar inverter. This AC power drives household appliances and, when combined with energy-saving plans, can meet most off-grid structure need.

Figure 5.1. Longi PV 550W module

The specification of PV panels used usually for such proposed system may include the following:

1. Monocrystalline
2. Front Cover 3.2 mm thermally pre-stressed glass with
3. anti-reflection technology
4. Back Cover Composite film
5. Frame Anodized aluminum
6. PV module min Efficiency 21%
7. Warranty 25 years

8. Each PV module used in any solar power project must use an RF identification tag (RFID)

Photovoltaic arrays necessitate installation on a stable and robust framework capable of both accommodating the array's weight and enduring challenging weather conditions such as wind and rain. The modules are affixed to structures with stationary configurations. The materials chosen for these structures are Hot dip Galvanized Mild Steel, conforming to IS 2062:1992, or aluminum of an appropriate grade, with a minimum alloy specification of 6063 or superior.

5.2. Solar Controller

A solar charge controller, known as a solar regulator, functions to regulate battery charging by connecting solar panels and the battery, preventing overcharging. These controllers have been integral to off-grid solar power systems for years and are vital for small-scale setups. Solar charge controllers come in two main types: PWM and MPPT. Pulse Width Modulation (PWM) controllers establish a direct link from the solar array to the battery and employ a 'rapid switch' approach to regulate battery charging. The transistor opens until the battery reaches its absorption charge voltage; it then rapidly switches on and off (hundreds of times per second) to maintain steady battery voltage. While effective, this method reduces the solar panel's operating voltage (Vmp), diminishing power output and efficiency. MPPT stands for Maximum Power Point Tracker, a more advanced version of the PWM charge controller. These controllers optimize solar panel performance at their peak power point, achieving the optimal voltage and current combination for maximum power output. They can enhance efficiency by up to 30% compared to PWM controllers, contingent on battery factors and the solar panel's Vmp (operating voltage).

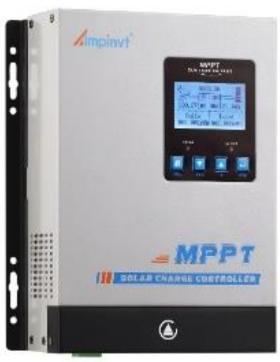

Figure 5.2. MPPT Solar Charge Controller

An MPPT, which stands for maximum power point tracker, is an efficient type of DC-to-DC converter utilized to enhance the power output of a solar system. Its operational principle is straightforward: due to the varying levels of sunlight exposure on a solar panel throughout the day, the panel's voltage and current continually fluctuate. To achieve optimal power generation, an MPPT scrutinizes the panel's voltage to identify the ideal balance of voltage and current that yields the maximum power output. This process involves ongoing tracking and adjustment of the photovoltaic (PV) voltage to generate the highest achievable power, irrespective of the time of day or prevailing weather conditions. Through the incorporation of this innovative technology, operational efficiency experiences a significant boost, leading to a potential energy production increase of up to 30% compared to a PWM charge controller.

5.3. VRF-Unit

VRF technology is ideal for applications with varying loads or where zoning is necessary due to its ability to adjust the amount of refrigerant sent to fan coil units throughout a building. It also provides design flexibility, energy conservation, and economical installation. Furthermore, VRF systems can be either heat pump systems or heat recovery systems when simultaneous heating and cooling are needed. In a VRF system, multiple indoor fan coil units can be connected to a single outdoor unit with one or more inverter-driven compressors that can adjust their speed by changing the frequency of the power supply.

Figure 5.3. Typical VRF Heat Pump System

The adjustment of the compressor speed directly affects the quantity of refrigerant dispensed, subsequently influencing the temperatures within the indoor units. Individual indoor fan coil units are outfitted with dedicated metering devices, which are controlled either by the indoor units or the outdoor unit. When a refrigerant request is sent by each indoor unit to the outdoor unit, the latter supplies the precise amount of refrigerant essential to satisfy the demands of every individual indoor unit. The Variable Refrigerant Flow (VRF) system is exceptionally suited for applications necessitating load adjustment in accordance with usage patterns or the building's orientation. It is also well-suited for applications requiring zoning capabilities.

Advantages of a VRF System:

1- Control Means Comfort: The best way to ensure a comfortable environment is to provide heating or cooling exactly when and where it is needed, without any sudden temperature changes. Traditional systems turn the compressor either completely on or off, resulting in unpredictable shifts in the temperature of a room, even if individual controls are in place (Figure. 5.4).

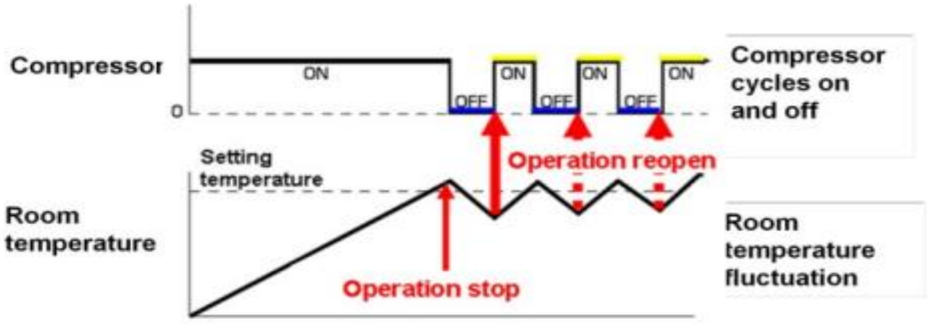

Figure 5.4. Traditional Fixed-Speed Compressor

A Variable Refrigerant Flow (VRF) system allows for the speed of the compressor to be adjusted, meaning that it does not turn on and off but runs continuously for extended periods (Fig. 5.5). This allows for the refrigerant flow to be adjusted to keep the room temperature consistent and maintain the desired comfort level. Furthermore, fan speeds and louver positions at the indoor units can be varied to further enhance the comfort of the space.

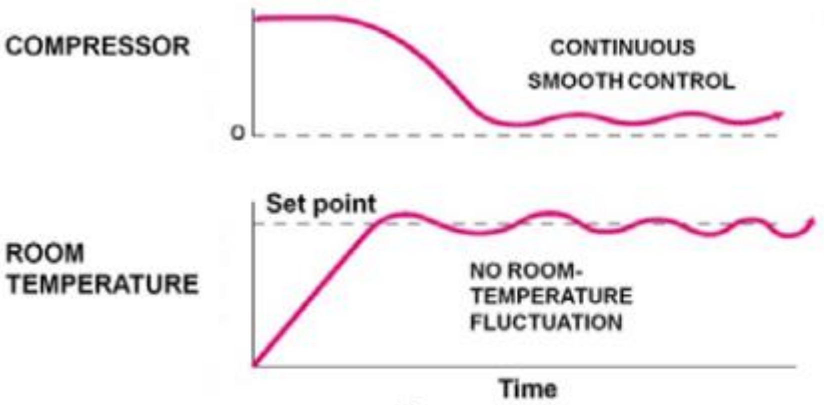

Figure 5.5. VRF System Inverter-Driven Compressor

2- Design Flexibility: A notable benefit of the VRF system lies in its capacity to offer design flexibility, facilitated by a wide range of product options. Diverse types and sizes of fan coils are at hand, ensuring suitability for various applications.

3- Cost-Effective Installation: A VRF system may be a great cost-saving option for certain applications. Its outdoor units are light and take up little space, so they can be transported in a service elevator and don't require the use of a crane for rooftop installation. Plus, the lightweight units don't call for extra support structures in the roof, which could potentially lead to further savings on construction costs.

4- Energy Savings: VRF systems offer energy savings by varying the compressor speed to match the output of the system to the load, eliminating the energy losses associated with systems that circulate conditioned air through ductwork. The efficiency of the system may depend on the design of the outdoor unit.

5.4. Cold Thermal Energy Storage

Cooling constitutes a substantial energy-intensive process, and cold thermal energy storage stands as a resourceful energy-saving technology capable of curtailing electricity consumption. This method encompasses the accumulation of cold thermal energy within a medium, subsequently extracting it for use as required. Throughout the charging phase, available cold thermal energy is amassed, and in the discharging phase, the stored cold thermal energy is accessed and supplied for practical utilization. This can be achieved by altering the internal energy of the storage medium or undergoing a phase transformation. By capitalizing on peak and off-peak periods, cold thermal energy storage technology facilitates the capture of cold during high-demand times and its release during low-demand periods, thereby optimizing energy usage.

Within the domain of cold thermal energy storage, two prevalent strategies are the sensible and latent storage approaches. Sensible heat storage capacity hinges on specific heat capacity and temperature changes, without any phase transition during energy storage and retrieval. Meanwhile, latent heat energy storage garners appeal due to its remarkable energy storage density, ranging from 5 to 14 times higher than the sensible storage method. This approach entails a phase alteration during both energy storage and retrieval. The stored energy quantity aligns with the material's latent heat of fusion.

The combination of Phase Change Materials (PCMs) and Thermal Energy Storage (TES) systems presents an opportunity to drastically improve energy efficiency in Heating, Ventilation, and Air Conditioning (HVAC) systems. PCMs are materials that have the capacity to store and release thermal energy when undergoing a phase change, transforming from solid to liquid, or liquid to solid. By incorporating PCMs into a TES tank, which contains a heat transfer fluid (HTF), electrical energy used to power HVAC systems is stored as latent thermal energy. This storage capability allows buildings to qualify for Net-Zero Energy in Buildings programs where energy is generated on-site and also provides a method of temporal decoupling of energy generation and energy use. Our proposed system utilizes Photovoltaic (PV) panels to generate electricity, which is then converted into thermal energy by a Variable Refrigerant Flow (VRF) unit. This thermal energy is then stored in a Phase Change Material (PCM) Tank for use during peak cooling periods when electricity prices are at their highest. This method of cooling the building eliminates the need for carbon-intensive and expensive peak power plants, which rely on burning fossil fuels to produce electricity, consequently reducing the carbon footprint associated with the process. As a result of this, energy can be accumulated when production costs and carbon discharges are high, and then used at a later point when the costs and atmospheric pollution are lower; this can be done during the day and night, resulting in financial savings as well as a reduction in energy and carbon emission levels.

The selection of n-pentadecane as an organic phase change cold storage material was a wise choice due to its ideal phase change temperature and remarkable cold storage capacity. This material has the capacity to store a large amount of energy, which makes it very efficient and cost-effective for energy storage purposes.

Table 5.1. Properties of N-Pentadecane PCM

Melting temperature	°C	8±1	Thermal conductivity	W/m.K	0.5
Latent heat of fusion L_f	KJ/Kg	180	Density	Kg/m3	862

Additionally, its low melting point allows it to be used in HVAC systems with minimal energy loss. This makes n-pentadecane an ideal material for cooling applications, as it ensures that the temperature requirements of the system are met without wasting energy. Furthermore, the material is highly resilient and requires minimal maintenance, ensuring that the system is running smoothly and efficiently. All of these factors make n-pentadecane an ideal choice for HVAC cold storage applications.

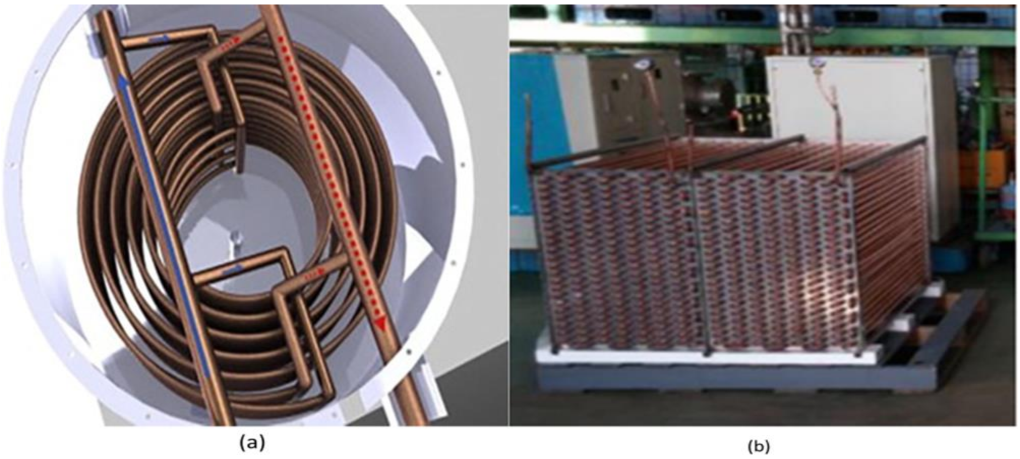

Figure 5.6. (a) coil-in-tank and (b) tube-in-tank CTES designs

The refrigerant circuit has been enhanced with two proposed designs for Cold Thermal Energy Storage (CTES), depicted in Figure 5.6: the coil-in-tank and tube-in-tank configurations. These designs incorporate one or multiple coils/tubes submerged within the Phase Change Material (PCM) storage tank. Over the past two decades, tanks containing macro-encapsulated PCM, like spheres and small capsules, have gained prominence as preferred options for CTES systems. In this setup, the refrigerant circulates within the tubes, engaging in heat exchange with the PCM. This interaction facilitates both the charging and discharging operations.

6. SIMULATION RESULTS

6.1. Load shifting Scenario

Figure 6.1 provides the hourly typical load profile. The peak loading of the conventional system occurs during the day when the internal thermal load, temperatures, and solar gain are higher. CTES system runs chilled water in the loop through FCU when needed.

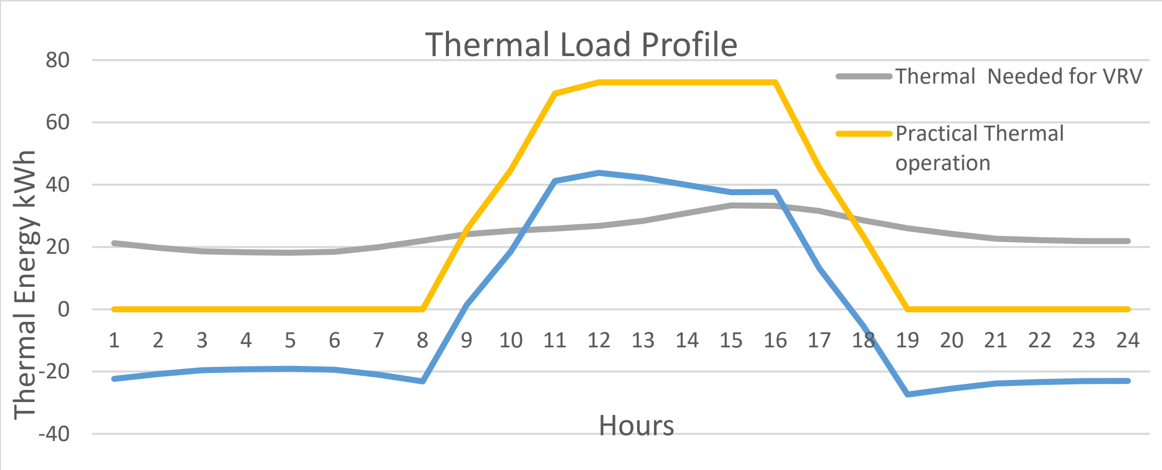

Figure 6.1. One Day Thermal load profile at peak load

The operation strategy for a Cold Thermal Energy Storage (CTES) integrated into a Variable Refrigerant Flow (VRF) cooling system is outlined. The scenario considers a fully charged storage undergoing simultaneous charging and discharging phases. In this setup, the storage has the capability to address the complete cooling load during peak hours. However, a high-capacity HVAC system is necessary to achieve complete CTES charging, intended for operation during off-peak hours. Both the storage capacity and the VRF system were meticulously designed to maintain a nearly constant load throughout an 8-hour period of sunlight. The storage capacity was engineered to encompass a 24-hour cooling capacity.

6.2. PV-Batteries-VRF

After implementing the energy mathematical model of the different components. The intent is to find the optimal combination between the solar panel number and the capacity of batteries capable of running the system year-round with all hourly auxiliary energy rate values $\dot{Q}_{aux}$ equal to zero with minimal capital cost. The optimization methodology is based on the Hooke and Jeeves algorithm in which the minimum initial values of the two variables are taken, then incremented by its research step value. The new values are then entered each time into the model which simulates the annual performance.

Since the main intent of this thesis study is to provide all the needed thermal loads from solar energy, the minimum number of panels was determined by dividing the total daily electric needed energy Q_T by the total daily energy Q_G generated at peak load using the area of one panel only at the optimal tilted angle (equals to the latitude of the city). The maximum number of panels is determined by the number of panels that could be installed over the available area in the residential village. The incremental step of the solar collectors is the number of panels.

As for the useful energy capacity, the minimum value was set to 1 kWh. The maximum value of the capacity was set to be the total annual thermal energy for 5 days storage.

Table 6.1 provides the minimum, maximum, incremental step, and the unit cost for the different components; cost includes the price of the PV panels, the price of the batteries storage, and all other installation costs like cables, steel structures, Inverter, and controls that collected from manufacturers and published papers for both models.

Table 6.1. Optimization Parameters for VRF-Batteries system

Parameter	Units	**Baseline**	**Optimized**
PV Area per panel	m^2/panel	2	
PV Minimum Number of Panels	Nb	60	48
PV Maximum Number of Panels	Nb	120	
PV Incremental step	Panel	1	
PV Optimal value	Panel	76	68
PV Unit cost per panel	USD/panel	110	
Minimum Useful Energy Value	kWh	1	
Maximum Useful Energy Value	kWh	500	
Incremental step useful Energy value	kWh	1	
Optimal useful energy value	kWh	88	79
Unit cost	USD/kWh	60	
Other installation unit costs (inverter, cables,..)	USD/Per PVpanel	100	

The search procedure takes place in two stages:

The first stage is to find all the configurations having a total annual auxiliary energy Q_{aux} equal to zero. For each PV panel within the boundary limitation (from minimum to maximum), the simulation analysis was performed with each value of the batteries capacity from the minimum limit value and incremental values up until zero auxiliary is reached. All the different combinations are summarized in Figures 6.2 and 6.3.

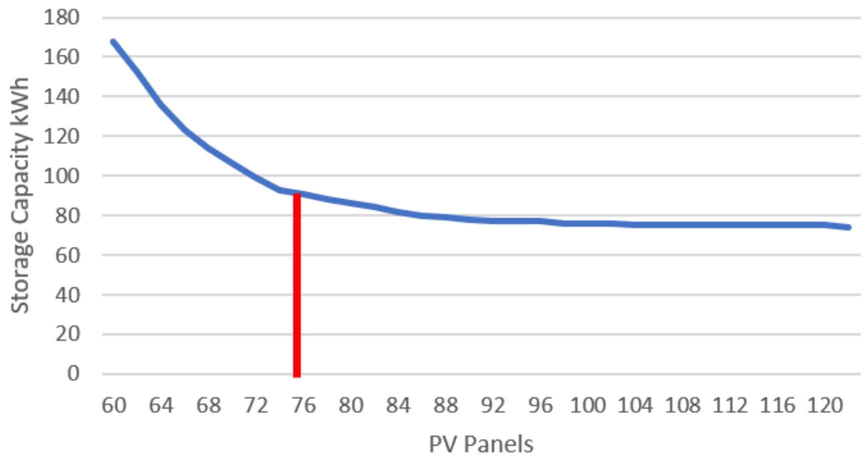

Figure 6.2. Batteries capacity depending on the number of PV panels for baseline model

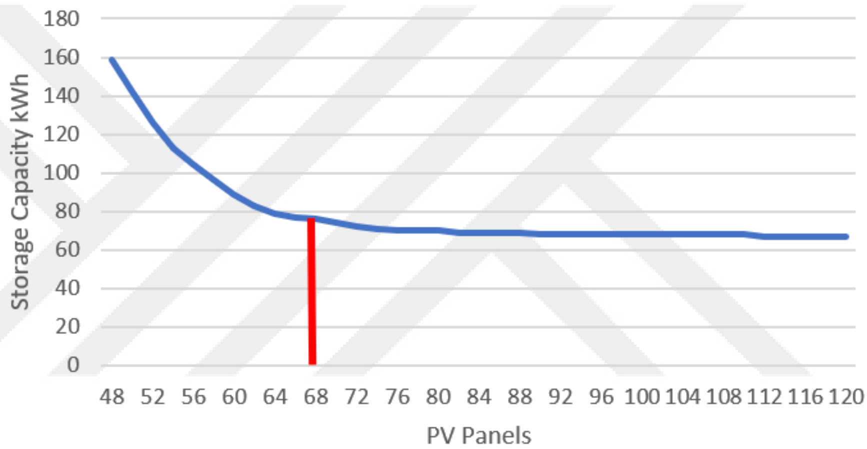

Figure 6.3. Batteries capacity depending on the number of PV panels for the optimized model

Figures 6.2 and 6.3 represent the capacity of batteries needed against the number of PV panels. And as predicted, while incrementing the number of PVs, the capacity of batteries will decrease. This is due to one factor; when the number of PVs increase, at daytime, the electrical load supplied by these will be sufficient to run the required cooling load without the usage of the batteries storage. However, an inflection point appears, and this point represents that adding more PVs will not add value to the system, because the storage is nearly decreasing. This is why for the Baseline model the number of Panels chosen was 76 and the capacity of batteries will be 88 kWh and for the Optimized model the number of Panels chosen was 68 and the capacity of batteries will be 76 kWh.

The second stage is based on finding the minimum initial cost between the different combinations. The capital cost of all the possible combinations having a solar fraction equal to 1 is summarized in Figures 6.4 and 6.5. Then the minimum value between them was chosen. And thus, the optimal operating schedule and the capacities of the different components were determined.

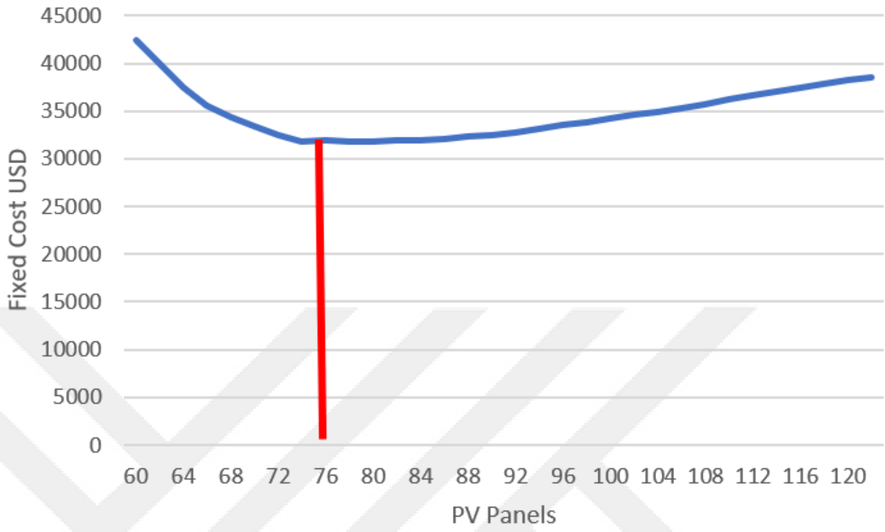

Figure 6.4. Cost of the System depending on the number of PV panels for baseline model

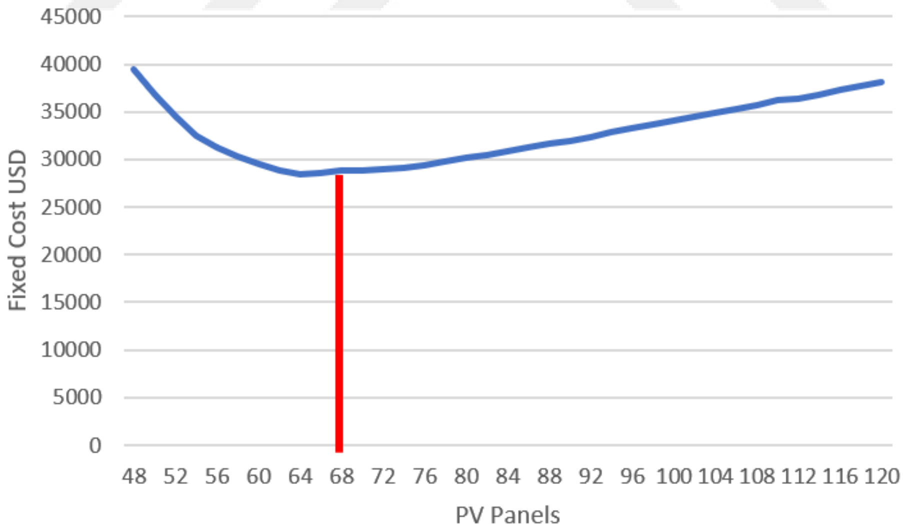

Figure 6.5. Cost of the System depending on the number of PV panels for optimized model

What was mentioned in the graphic before is illustrated in Figures 6.4 and 6.5. At the inflection point, increasing the number of PVs will mean oversizing the system, and the cost will increase with no advantage added to the system. Therefore, the system will cost around 31,800$ for LBV and 29,370$ for OPV in case of using batteries. These number is the summation of PV Panels with their installation, Batteries, Inverter, Optimization cost in OPV, cables, and all other accessories, taking into consideration the profit of the contractor.

6.3. PV-PCM-VRF

After implementing the energy mathematical model of the different components. The intent is to find the optimal combination between the solar panel number and the capacity of PCM storage capable of running the system year-round with all hourly auxiliary energy rate values $\dot{Q}_{aux}$ equal to zero with minimal capital cost. The optimization methodology is based on the Hooke and Jeeves algorithm in which the minimum initial values of the two variables are taken, then incremented by its research step value. The new values are then entered each time into the model which simulates the annual performance.

Since the main intent of this thesis study is to provide all the needed thermal loads from solar energy, the minimum number of panels was determined by dividing the total daily needed thermal cooling energy $Q_{cooling,needed}$ by the total available cooling energy $Q_{cooling,available}$ generated at peak load using the area of one panel only at the optimal tilted angle (equals to the latitude of the city). The maximum number of panels is determined by the number of panels that could be installed over the available area in the residential village. The incremental step of the solar panel is one panel.

As for the PCM cold storage volume, the minimum value was set to 1 Liter. The maximum value of the capacity was set to be volume compared to total annual thermal energy. The incremental step value of the PCM storage is set to 25 Liters which is equivalent to 1 kWh of cold thermal storage.

Table 6.2. Optimization Parameters for VRF-PCM system

Parameter	Units	**Baseline**	**Optimized**
PV Area per panel	m^2/panel	2	
PV Minimum Number of Panels	Nb	60	48
PV Maximum Number of Panels	Nb	120	
PV Incremental step	Panel	1	
PV Optimal value	Panel	70	62
PV Unit cost per panel	USD/panel	110	
Minimum PCM Volume	liter	1	
Maximum PCM Volume	liter	30000	
Incremental step PCM Volume	liter	25	
Optimal PCM Volume	liter	10376	9801
Unit cost	USD/liter	0.75	
Other installation unit cost (Cables, pipes, etc.)	USD/Per PV panel	80	
VRF price difference between Conventional and New system	USD	2000	

Table 6.3 provides the minimum, maximum, incremental step, and all the unit costs for the different components; cost includes the price of the PV panels, PCM storage, VRF price difference between Conventional and New systems, and all other installation costs like cables, steel structures, chilled water pipes and controls that collected from manufacturers or published papers.

The search procedure takes place in two stages, The first stage is to find all the configurations having a total annual auxiliary energy Q_{aux} equal to zero. For each PV panel within the boundary limitation (from min to maximum), the simulation analysis was performed with each value of the PCM's capacity from the minimum limit value and incremental values up until zero auxiliary is reached. All the different combinations are summarized in the following graphs:

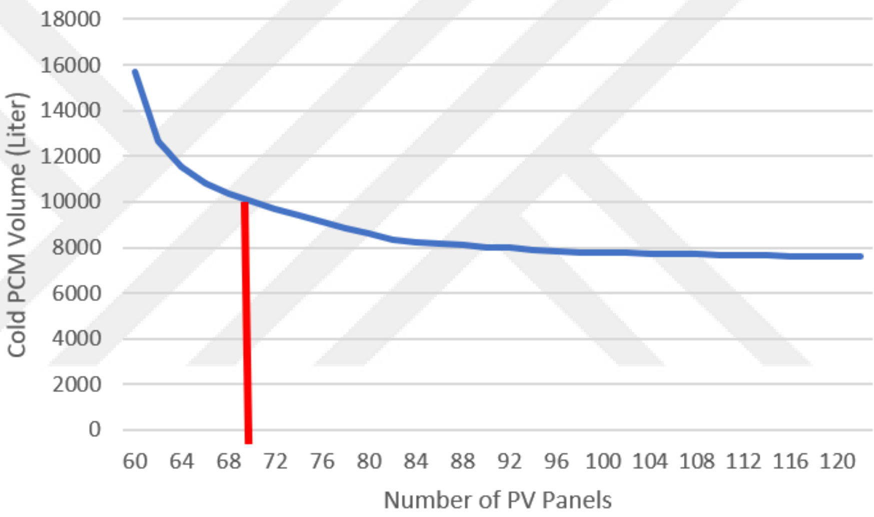

Figure 6.6. PCM Cold Storage depending on the number of PV panels for baseline model

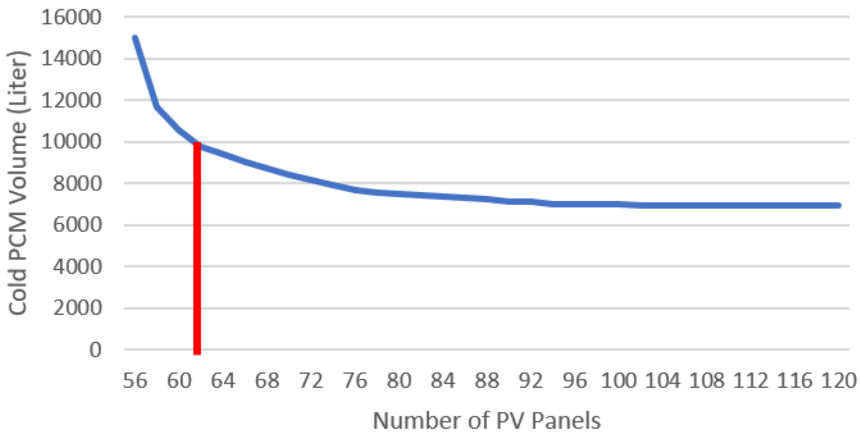

Figure 6.7. PCM Cold Storage depending on the number of PV panels for optimized model

Figures 6.6 and 6.7 represent the capacity of Cold PCM volume needed against the number of PV Panels. And as predicted, while incrementing the number of PVs, the capacity of cold PCM storage will decrease. This is due to one factor; when the number of PVs increase, at daytime, the electrical load supplied by these will be sufficient to run the required cooling load without the usage of the thermal storage. However, an inflection point appears, and this point represents that adding more PVs will not add value to the system, because the storage is nearly decreasing. This is why for the Baseline model the number of Panel chosen was 70 and the capacity of PCM storage will be 10,376 L and for the Optimized model the number of Panel chosen was 62 and the capacity of PCM storage will be 9,801 L.

The second stage is based on finding the minimum initial cost between the different combinations. The capital cost of all the possible combinations having a solar fraction equal to 1 is summarized in the following graph.

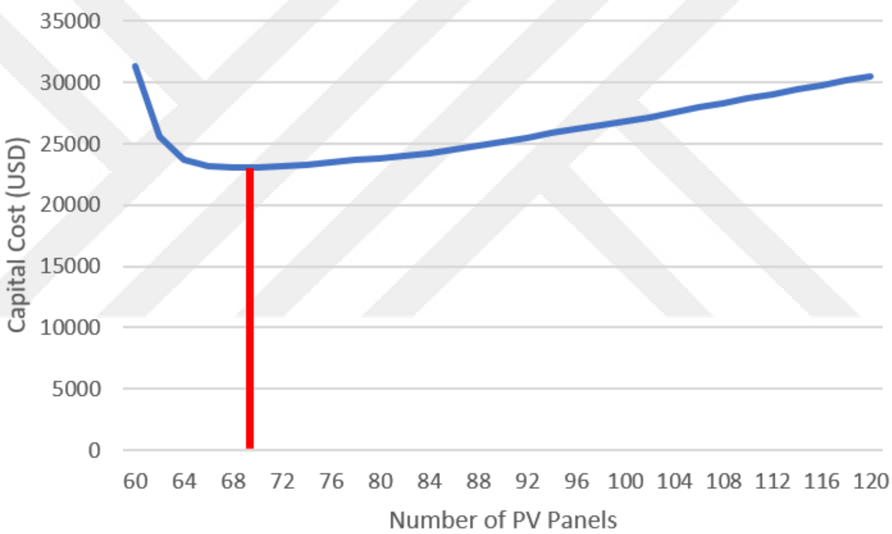

Figure 6.8. Cost of the System depending on the number of PV panels in baseline model

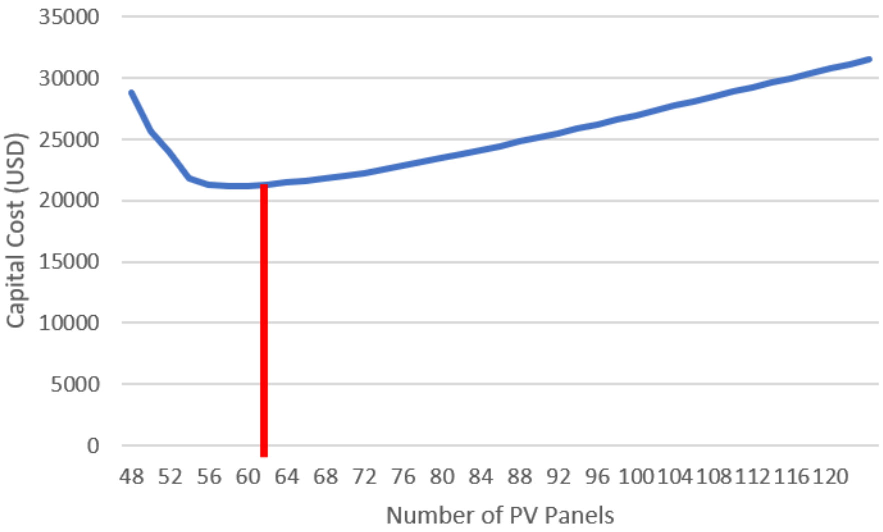

Figure 6.9. Cost of the System depending on the number of PV panels in optimized model

What was mentioned in the graphic before, is illustrated in Figures 6.8 and 6.9. At the inflection point, increasing the number of PVs will mean oversizing the system, and the cost will increase with no advantage added to the system. Therefore, the system will cost around 23,082$ for LBV and 22,001$ for OPV in case of using PCM cold thermal storage. This number is the summation of PV Panels with their installation, PCM storage, Inverter, Optimization cost in OPV, cables, and all other accessories, taking into consideration the profit of the contractor.

7. FEASIBILITY STUDY

The pricing of various components and the associated maintenance costs for both systems are sourced from market operators and manufacturers. The initial investment cost is calculated as the disparity between the initial expenses of the novel solar system and the conventional Variable Refrigerant Flow (VRF) system that could have been employed instead. Earnings are determined as the discrepancy between the electricity bills paid within the conventional system and those projected with the utilization of the new solar system.To offer clarity regarding the conducted feasibility study, certain parameters warrant elucidation. The Discountable Net Present Value (NPV) signifies the cumulative sum of profit accrued at the conclusion of the investment's lifespan. It is founded on the real values of earnings and expenses, as computed in Equation (7.1) and Equation (7.2):

$$VA = \frac{VF}{(1+i)^n} \tag{7.1}$$

$$NPV = \sum VA(Earnings) - \sum VA(Expenses) - (Investment - Subsidies) \tag{7.2}$$

Where $\sum VA(Earnings)$ and $\sum VA(Expenses)$ are respectively the sum of actual values of earnings and expenses. n is the lifetime duration of the system and i is the discount rate per period in each country. VF are the future values.

The Internal Rate of Return IRR is the value of the interest rate such that the NPV is zero. It is calculated using an iterative function. If IRR is greater than the hurdle rate, the project is more profitable.

The Profitability Index PI (or Return on Investment ROI) calculated in Eq. (36) give the sign on how much a system is profitable. The more this value, the higher the system is profitable.

$$PI = \frac{\sum VA(Earnings) - \sum VA(Expenses)}{Investment - Subsidies} \tag{7.3}$$

The Actual Payback Period is then calculated after finding the actual cash flow year by year as shown in Eq. (37) and Eq. (38):

$$ACF_t = -[ACF_{t-1} - (VA_t(Earnings) - VA_t(Expenses))] \tag{7.4}$$

$$ACF_0 = -[Investment - Subsidies] \tag{7.5}$$

Where ACF_t is the actual cash flow at year "t". Then the year t, where the actual cash flow changes sign and becomes a positive value, is the payback period of the system.

For the conventional system Tables 7.1 and 7.2 and Figures 7.1 and 7.2 provide all the financial inputs parameters and results are calculated using present discounted cash inflows which take into consideration the time value of money. As stated, the unit cost for this system includes the price of the PV panels, the price of the batteries storage multiplied by 3 considering the storage will be renewed 3 times during the lifetime period, and installation cost (cables, steel structures, Inverter, etc.). As for the optimized model, an optimization cost will be added which is the cost difference between the single glassing and double glassing.

Table 7.1. VRF-Batteries System Feasibility Study Parameters for LBV

Financial Parameters		Subsidized Price	Production Real Price
Investment	USD	31800	31800
Electricity Saving	kWh	20762	20762
Price per kWh	USD	0.16	0.32
Earnings per year	USD	3322	6644
Expenses per year	USD	200	200
Net Present Value NPV	USD	1703	37353
IRR	%	9.8%	23.5%
PI	-	1.05	2.17
Actual Present Value Payback period=	Years/Months	13 years 12 Months	5 years 11 Months

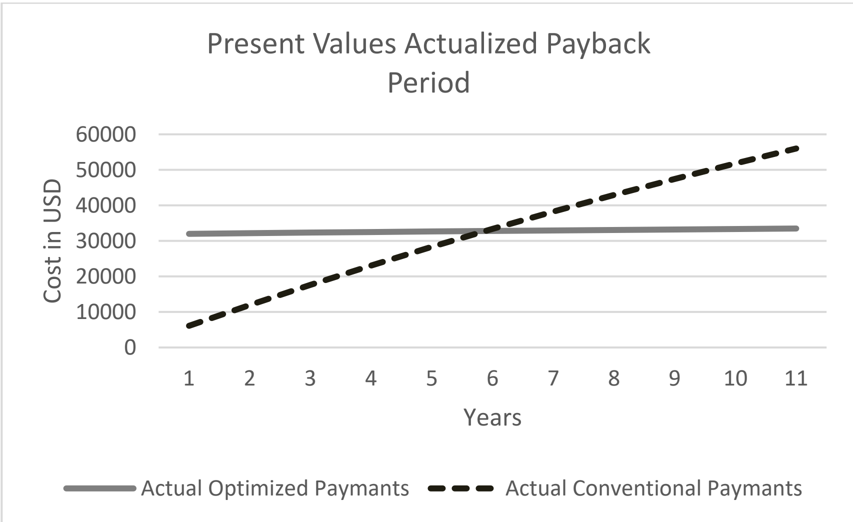

Figure 7.1. Present Values Actualized Payback Period for LBV

Table 7.2. VRF-Batteries System Feasibility Study Parameters for OPV

Financial Parameters		Subsidized Price	Production Real Price
Investment	USD	29370	29370
Electricity Saving	kWh	20762	20762
Price per kWh	USD	0.16	0.32
Earnings per year	USD	3322	6644
Expenses per year	USD	200	200
Net Present Value NPV	USD	4133	39783
IRR	%	11.0%	25.4%
PI	-	1.14	2.35
Actual Present Value Payback period=	Years/Months	12 years 8 Months	5 years 5 Months

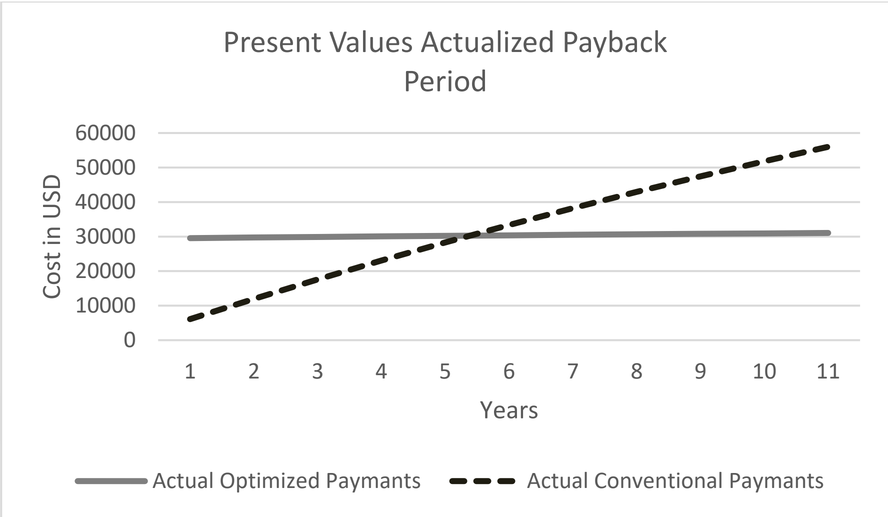

Figure 7.2. Present Values Actualized Payback Period for OPV

For the proposed system Tables 7.3 and 7.4 and Figures 7.3 and 7.4 provide all the financial inputs parameters and results are calculated using present discounted cash inflows which take into consideration the time value of money. As stated, the unit cost for this system includes the price of the PV panels, the price of the PCM storage, and installation cost (cables, steel structures, Inverter…etc) In addition the consumption of the chilled water pump was calculated and subtracted from the annual electricity saving. As for the optimized model, an optimization cost will be added which is the cost difference between the single glassing and double glassing.

Table 7.3. VRF-PCM System Feasibility Study Parameters for LBV

Financial Parameters		Subsidized Price	Production Real Price
Investment	USD	23082	23082
Electricity Saving	kWh	20372	20372
Pump consumption	kWh	390	390
Price per kwh	USD	0.16	0.32
Earnings per year	USD	3260	6519
Expenses per year	USD	200	200
Net Present Value NPV	USD	9756	44730
IRR	%	14.8%	31.4%
PI	-	1.42	2.94
Actual Present Value Payback period=	Years/Months	9 years 7 Months	4 years 3 Months

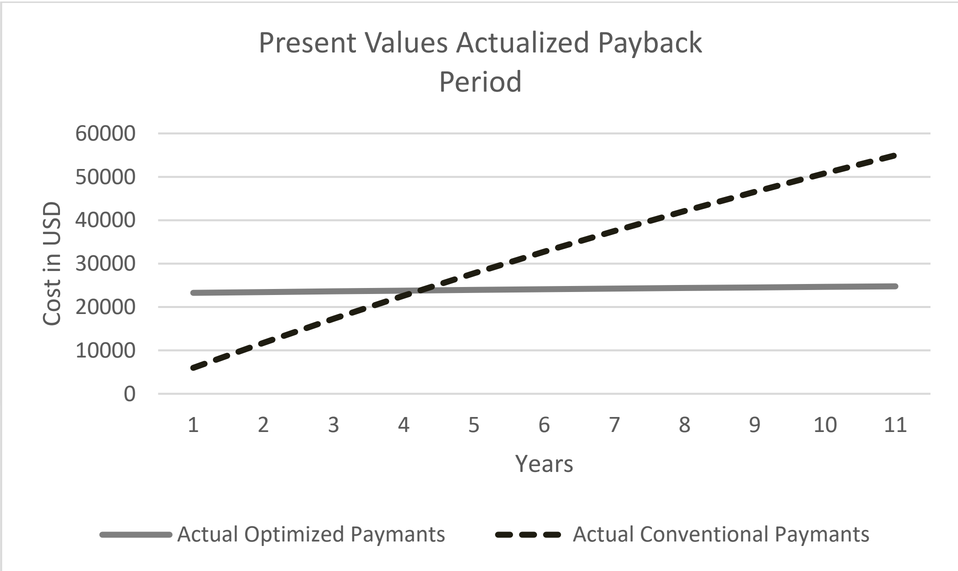

Figure 7.3. Present Values Actualized Payback Period for LBV

Table 7.4. VRF-PCM System Feasibility Study Parameters for OPV

Financial Parameters		Subsidized Price	Production Real Price
Investment	USD	22001	22001
Electricity Saving	kWh	20412	20412
Pump consumption	kWh	350	350
Price per kwh	USD	0.16	0.32
Earnings per year	USD	3260	6519
Expenses per year	USD	200	200
Net Present Value NPV	USD	12887	47936
IRR	%	16.8%	33.8%
PI	-	1.59	3.18
Actual Present Value Payback period=	Years/Months	8 years 5 Months	3 years 11 Months

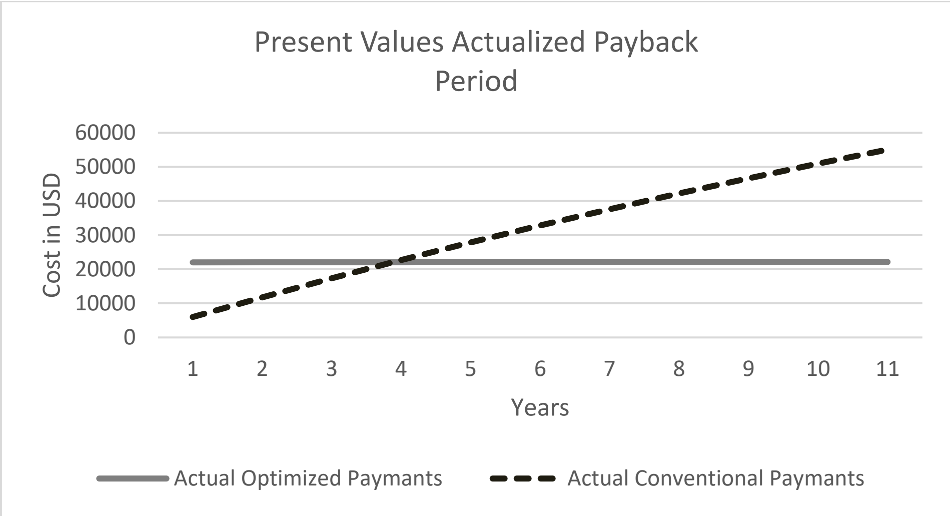

Figure 7.4. Present Values Actualized Payback Period for OPV

8. RESULTS ANALYSIS

After running the optimization simulation and conducting a feasibility study on all possible systems and cases, a conclusion was drawn that will help in identifying the best possible system and the most suitable case for the study. The electrical tariff in Türkiye is highly subsidized, the residential tariff is 0.16 USD/kWh. Thus, the payback period of the solar cooling system was found to be relatively high. However, the energy policy in Türkiye is tending towards eliminating these subsidies, resulting in a residential tariff of 0.30 USD/kWh which was used in our feasibility study. The baseline model results for the PV-Batteries system showed that 76 PV panels with 88kWh batteries storage capacity were needed, 31800$ investment cost with an actual present value payback period of 5 years and 11 months, PI of 2.17 and IRR of 23.5%. While results for the PV-PCM-VRF system showed that 70 PV panels with 10376 litters PCM storage capacity were needed, 23082$ investment cost, with an actual present value payback period of 4 years, and 3 months, PI of 2.94 and IRR of 31.4%. The PV-PCM-VRF system has an investment cost of 23,082$ compared to 31,800$ for the PV-Batteries system, resulting in a 27.41% cost savings. Additionally, the PV-PCM system has a payback period of 4 years and 3 months compared to 5 years and 11 months for the PV-Batteries system, resulting in a 23% reduction in the payback period. Furthermore, the PV-PCM system has an Internal Rate of Return (IRR) of 31.4%, while the PV-Batteries system has an IRR of 23.5%, resulting in a 33.6% increase in the IRR. Although results obtained have shown that adopting a 100% solar fraction system will enhance the profitability by only around 35.5%. Thus, the PV-PCM system results in an investment cost that is lower than the PV-Batteries system and also a shorter actual present value payback period, and a higher IRR.

As For the optimized model: the PV-Batteries system result was found 68 PV panels with 79 kWh batteries storage capacity,29,370$ investment cost, with actual present value payback period of 5 years and 5 months, PI of 2.35 and IRR of 25.4% while the PV-PCM system result was found 62 PV panels with 9801 litters PCM storage capacity 22,001$ investment cost with actual present value payback period of 3 years and 11 months, PI of 3.18 and IRR of 33.8%. Therefore, the PV-PCM system provides a lower cost of investment and a shorter payback period than the PV-Batteries system. The PV-PCM system has an investment cost of 22,001$ compared to 29,370$ for the PV-Batteries system, resulting in a 24.4% cost savings. Additionally, the PV-PCM system has a payback period of 3 years and 11 months compared to 5 years and 5 months for the PV-Batteries system, resulting in a 27.3% reduction in the payback period. Furthermore, the PV-PCM system has an Internal Rate of Return (IRR) of 33.8%, while the PV-Batteries system has an IRR of 25.4%, resulting in a 32.3% increase in the IRR. Although results obtained have shown that adopting a 100% solar fraction system will enhance the profitability by only around 35.3%. Thus PV-PCM system results in an investment cost that is lower than the PV-Batteries system and also a shorter actual present value payback period and a higher IRR.

Therefore, the PV-PCM-VRF system compared to the PV-Batteries system in both models is a more cost-efficient and profitable option for solar energy storage compared to the PV-Batteries system. Accordingly, we were able to conclude that when it comes to effectiveness, durability, capital investment, price, and economic benefits, PCM is deemed to be more convent than using batteries as energy storage instruments.

By comparing the conventional system in both models, the baseline model required 76 PV panels with 88kWh batteries storage capacity, an investment cost of 31800$, a payback period of 5 years and 11 months, a PI of 2.17, and an IRR of 23.5%.While the optimized model required 68 PV panels with 79kWh batteries storage capacity, an investment cost of 29370$, a payback period of 5 years and 5 months, a PI of 2.35, and an IRR of 25.4%. Results obtained show that adopting the optimization enhancements of the energy conservation and efficiency measures cause a reduction of 11% in PV panels and 10% in batteries storage capacity, 8.3% in investment cost, 5.2% in payback period, enhancing 8.2% in IRR and the profitability index by around 8.2% if compared to the local baseline model.

By comparing the proposed system in both models, we found that the baseline model required 70 PV panels with 10376 litters PCM storage capacity, 23082$ investment cost, an actual present value payback period of 4 years, and 3 months, a PI of 2.94 and IRR of 31.4%. While as for the optimized model results was found 62 PV panels with 9801 litters PCM storage capacity of 22,001$ investment cost with an actual present value payback period of 3 years and 11 months, PI of 3.18, and IRR of 33.8%. Results obtained show that adopting the optimization enhancements of the energy conservation and efficiency measures cause a reduction of 11.5% in PV panels and 6.3% in PCM storage capacity, 3.07% in investment cost, 8.8% in payback period, enhancing 7.7% in IRR and profitability index by around 8.1% if compared to the local baseline model.

Accordingly, we were able to conclude that when it comes to effectiveness, durability, capital investment, price, and economic benefits, PCM is deemed to be more convent in both models than using batteries as energy storage technologies especially after analyzing the results of the optimization simulation and conducting a thorough feasibility study for all the possible systems and cases. Our optimization process has provided valuable insight into the effectiveness of the proposed system, allowing it to make informed decisions on which systems to implement.

9. CONCLUSION

Renewable energy is sourced from natural sunlight which will never run out, unlike more traditional energy-producing sources like coal and gas. According to scientists, systems based on renewable energy are set to account for almost 95% of the increase in global power capacity with solar PV alone providing for more than half.

This study provides a design guideline for creating, optimizing, and forecasting the performance of a 100% solar cooling system in any Mediterranean climate similar to Adana (Türkiye). With the use of the simulation application "Design Builder," a baseline and optimized model was created to generate the hourly cooling demands over the course of a year. The annual cooling load was found to be 83051 kWh and 74304 kWh for LBV and OPV respectively. The "Visual Basic" programming was used to create the mathematical model of various components, such as the photovoltaic panels, variable refrigerant volume units, and the cold phase change material. Using the Hooke and Jeeves optimization approach with the restriction of reaching a 100% solar fraction at the lowest initial cost.

Energy conservation and efficiency measures were adopted to reduce cooling thermal needs for the residential villa. A parametric study was performed to reveal the reduction percentage for each enhancement and then determine the overall hourly thermal energy profiles for the optimized villa (OPV). Within the scope of this study, results obtained show that adopting the optimization enhancements of the energy conservation and efficiency measures as for the conventional system(PV-Batteries-VRF) caused a reduction of 11% in PV panels, and 10% in batteries storage capacity, 8.3% in investment cost, 5.2% in payback period, enhancing 8.2% in IRR and the profitability index by around 8.2% if compared to the local baseline model. The proposed system (PV-PCM-VRF) cause a reduction of 11.5% in PV panels and 6.3% in PCM storage capacity, 3.07% in investment cost, 8.8% in payback period, enhancing 7.7% in IRR and profitability index by around 8.1% if compared to the local baseline model.

An optimization methodology was developed to find the best thermo-economical combination between the number of solar panels, and cold thermal PCM storage volume. The best thermo-economic combination was found to be 62 PV solar collectors, 66 kW VRF unit, and 9.801 m3 cold phase change material thermal storage. Since the electricity tariff is subsidized, the feasibility study shows that the payback period of this system is 8 years and 5 months if compared to the baseline conventional system of VRF units running using municipality electricity. Nevertheless, in keeping with the country's energy policy trend of eliminating these subsidies and utilizing the production cost, the payback period turns out to be 3 years and 11 months. The internal rate of return has reached 33.8% with a net present value of 47,936 USD.

It is revealed from the study that the proposed residential building's solar cooling system has the best benefits for the end-user consumer, government, and the world. If compared to the LBV, it would reduce annual electrical energy use, electricity costs, and CO2 emissions by 98%, Moreover, the research has shown that the installation of the PV system reduces approximately 8 tons of CO_2 yearly, incentivizing decision-makers to invest more in such systems.

Despite the high installation cost of the PV-driven VRF system and the fact that it is weather dependent, the use of solar energy proves to have an immense and powerful impact on the environment, especially when it comes to the universe's global warming crisis. In addition, a few years after its installation, it will certainly be seen as a way of reducing energy bills and electricity loss during long-distance transport.

The reason behind the present project and the completion of this report are to develop a clear and detailed comparison between different storage systems required for the establishment of a renewable energy system for a residential villa in Adana, Türkiye. This allowed us to set side by side the traditionally used storage system and the new more developed and innovative one and to decide on the more reliable system when it comes to the consumer's best interests.

Accordingly, we were able to conclude that when it comes to effectiveness, durability, capital investment, price, and economic benefits, PCM is deemed to be more convent than using batteries as energy storage instruments.

REFERENCES

A Glimpse at Our Possible Future Climate, Best to Worst Case Scenarios. (2013, February 13). Retrieved from http://skepticalscience.com/print.php?n=1866

Aguilar, F. J., Aledo, S., & Quiles, P. V., (2017). Experimental analysis of an air conditioner powered by photovoltaic energy and supported by the grid. Applied Thermal Engineering,123, 486-497

Amarnath, K. R.,(2009). Variable refrigerant flow: Demonstration of efficient space conditioning technology using variable speed drives. 13th European Conference on Power Electronics and Applications (pp. 1-10). IEEE.

American Society of Heating, Refrigerating and Air-Conditioning Engineers (ASHRAE). Energy-Efficient Design of Low-Rise Residential Buildings Standard 90.2-201, https://www.techstreet.com/ashrae/standards/ashrae-90-2-2018?product_id=2030773.

American Society of Heating, Refrigerating and Air-Conditioning Engineers (ASHRAE). Ventilation For Acceptable Indoor Air Quality Standard 62.1-2016, https://www.techstreet.com/ashrae/standards/ashrae-62-1-2016?product_id=1938421.

American Society of Heating, Refrigerating and Air-Conditioning Engineers (ASHRAE). International Weather for Energy Calculations (IWEC), V 2.0, 2012, https://www.techstreet.com/ashrae/standards/international-weather-for-energy-calculations-2-0-iwec-weather-files-dvd?product_id=1823067

Atallah, G. Possible Usage of Variable Refrigerant Flow in Arid Climate: Technical and Management Perspective. Engineering Management 2022, Qatar University, Doha, Qatar

Beck, M., Müller, K., & Arlt, W., (2016). Storing surplus solar energy in low temperature thermal storage for refrigeration applications. Energy and buildings, 122, 192-198.

Bilgili, M.,(2011). Hourly simulation and performance of solar electric-vapor compression refrigeration system. Solar Energy, 85(11), 2720-2731.

Buonomano, A., Calise, F., d’Accadia, M. D., Ferruzzi, G., Frascogna, S., Palombo, A., ... & Scarpellino, M., (2016). Experimental analysis and dynamic simulation of a novel high-temperature solar cooling system. Energy conversion and management, 109, 19-39.

Climate Change and Health Retrieved from https://www.who.int/news-room/fact-sheets/detail/climate-change-and-health

Ekici, B. B., (2015). Evaluation of TS 825 Thermal Insulation Requirements in Buildings in Terms of Solar Radiation. Megaron, 10(1), 14.

Gayapershad, R., & Inambao, F. L., (2021). Sizing and Cost Analysis of Solar PV Panel Arrays for an Off-Grid DC-Air Conditioner for a Testing Facility at Mangosuthu University of Technology (South Africa). International Journal of Renewable Energy Research, 11(1), 248-258.

Ghosh, S., & Yadav, R.,(2021). Future of photovoltaic technologies: A comprehensive review. Sustainable Energy Technologies and Assessments, 47, 101410.

Gilani, H. A., Hoseinzadeh, S., Karimi, H., Karimi, A., Hassanzadeh, A., & Garcia, D. A., (2021). Performance analysis of integrated solar heat pump VRF system for the low energy building in Mediterranean island. Renewable Energy, 174, 1006-1019.

Hu, L., Liu, Y., Wang, D., Luo, X., & Liu, H., (2022). Feasibility analysis and feature comparison of cold thermal energy storage for off-grid PV air-conditioned buildings in the tropics. Energy Conversion and Management, 254, 115176.

Hussein, H. A., Numan, A. H., & Kuder, K. M.,(2020). Solar Photovoltaic Direct-Driven Air Conditioning System Performance in Iraq. Engineering and Technology Journal, 38(7), 984-991.

IPCC Assessment Report., (2007). Retrieved from http://www.ipcc.ch/report/ar5/wg1/

IPCC Assessment Report., (2022). Retrieved from https://www.ipcc.ch/report/sixth-assessment-report-working-group-ii/

IPCC climate report 2022 summary: The key findings Retrieved from https ://climate .selectra.com/en/news/ipcc-report-2022

Istanbul Climate Retrieved from https://weatherspark.com/y/95434/Average-Weather-in-%C4%B0stanbul-Turkey-Year-Round.

Jaiswal, A. K., Mitra, S., Dutta, P., Srinivasan, K., & Murthy, S. S., (2016). Influence of cycle time and collector area on solar driven adsorption chillers. Solar Energy, 136, 450-459.

Khlifi, M. A., & Slimene, M. B.,(2021). Efficient off grid solar powered DC air conditioning system. Przegląd Elektrotechniczny, 97.

Kılıç, U., & Kekezoğlu, B., (2022). A review of solar photovoltaic incentives and Policy: Selected countries and Turkey. Ain Shams Engineering Journal, 13(5), 101669.

Koppen Climate Classification for Adana Retrieved from https://www.weatherbase.com/weather/weather summary.php3? s=6071 & city name=Adana,+Turkey.

Lee, J. H., Im, P., & Song, Y. H.,(2018). Field test and simulation evaluation of variable refrigerant flow systems performance. Energy and Buildings, 158, 1161-1169.

Li, Y., Zhao, B. Y., Zhao, Z. G., Taylor, R. A., & Wang, R. Z., (2018). Performance study of a grid-connected photovoltaic powered central air conditioner in the South China climate. Renewable energy, 126, 1113-1125.

Liu, Z., Li, A., Wang, Q., Chi, Y., & Zhang, L., (2017). Performance study of a quasi-grid-connected photovoltaic powered DC air conditioner in a hot summer zone. Applied Thermal Engineering, 121, 1102-1110.

Mateus, T., & Oliveira, A. C., (2009). Energy and economic analysis of an integrated solar absorption cooling and heating system in different building types and climates. Applied energy, 86(6), 949-957.

Mohammed, O. H., & Al-Salmany, Z. T., (2022). Performance Optimization of Solar PV System Utilized for Cooling System. EAI Endorsed Transactions on Energy Web, 9(39), e5-e5.

Opoku, R., Mensah-Darkwa, K., & Muntaka, A. S., (2018). Techno-economic analysis of a hybrid solar PV-grid powered air-conditioner for daytime office use in hot humid climates–a case study in Kumasi city, Ghana. Solar Energy, 165, 65-74.

Rahdar, M. H., Emamzadeh, A., & Ataei, A., (2016). A comparative study on PCM and ice thermal energy storage tank for air-conditioning systems in office buildings. Applied Thermal Engineering, 96, 391-399.

Schex, Richard & Krönauer, Andreas & Loistl, Felix & Korth, Timo & Schweigler, Christian & Remy, Michael & Linn, Johannes., (2017). Solar-Electric Driven Heating and Cooling System with PCM-Storage for Improved Grid Connection. 1-12. 10.18086/swc.28.16.

Syed, A., Izquierdo, M., Rodriguez, P., Maidment, G., Missenden, J., Lecuona, A., & Tozer, R., (2005) A novel experimental investigation of a solar cooling system in Madrid. International Journal of refrigeration, 28(6), 859-871

Topcu, S., Dilmac, S., & Aslan, Z., (1995). Study of hourly solar radiation data in Istanbul. Renewable energy, 6(2), 171-174.

TS 825 Thermal Insulation Requirements in Buildings in Turkiye, Thermal insulation requirements for buildings, May 2008, https://sayfam.btu.edu.tr/upload/dosyalar/1458664642TS-825_Standard.pdf

Turkey 2021 Energy Policy Review Retrieved from https://www.iea.org/reports/turkey-2021

Turkey CO2 Emission Reduction Target Retrieved from https://caneurope.org /turkey_2030 _targets/

Zhou, Y. P., Wu, J., Wang, R. Z., & Shiochi, S.,(2017). Energy simulation in the variable refrigerant flow air-conditioning system under cooling conditions. Energy and Buildings, 39(2), 212-220.

CURRICULUM VITAE

Ahmad ITANI, has graduated from Rafic Al-Hariri Official Secondary School. Then, received BE in Mechanical Engineering with an excellent GPA with honor from The International University of Beirut -BIU. I have been granted a scholarship from Türkiye Burslari (YTB) to study in one of the most prestigious universities in the world. My first internship was at EMTECH from August 2019 -September 2020 as a site Mechanical Engineering where I learned how to apply methods of fluids, thermodynamics & HVAC. I’ve also enrolled in plenty of workshops which were online and offline like HVAC, Plumbing, Firefighting and Water Supply design. Recently I am doing my full-time training program at Consult S.A.R.L as a Mechanical Design Engineer which is an engineering firm specialized in Electro-mechanical Design and Consultancy.

APPENDICES

ANNEX. 1 OPTIMIZATION ALGORITHM

A. Interface

Based on the mathematical modeling, a VRF PCM system calculator is programmed using "Visual Basic" Programming. This calculator consists of 2 pages:

1. System Input Page: represents the inputs page of the project's location, hourly site information, hourly building's cooling loads, total annual conventional electrical consumption, solar panels areas, tilt angle of the solar panels, cooling loads power, and phase change material energy capacity.

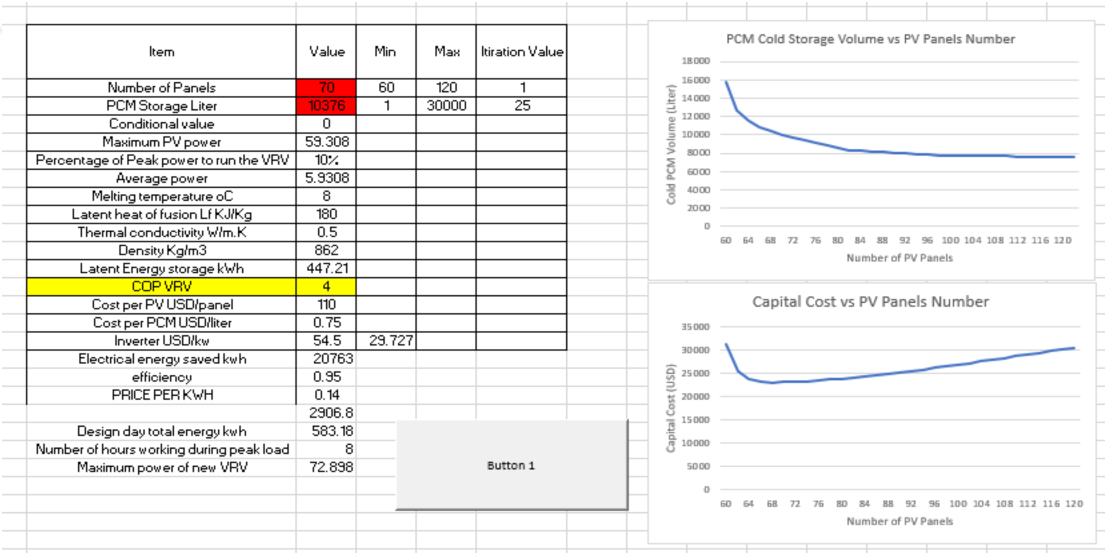

Item	Value	Min	Max	Itiration Value
Number of Panels	70	60	120	1
PCM Storage Liter	10376	1	30000	25
Conditional value	0			
Maximum PV power	59.308			
Percentage of Peak power to run the VRV	10%			
Average power	5.9308			
Melting temperature oC	8			
Latent heat of fusion Lf KJ/Kg	180			
Thermal conductivity W/m.K	0.5			
Density Kg/m3	862			
Latent Energy storage kWh	447.21			
COP VRV	4			
Cost per PV USD/panel	110			
Cost per PCM USD/liter	0.75			
Inverter USD/kw	54.5	29.727		
Electrical energy saved kwh	20763			
efficiency	0.95			
PRICE PER KWH	0.14			
	2906.8			
Design day total energy kwh	583.18			
Number of hours working during peak load	8			
Maximum power of new VRV	72.898			

Figure 8. Optimized page in Excel

2. Optimized Page: it consists of one buttons. The "Loop run" runs an iterative function that finds for each solar panel number its coincident PCM thermal energy storage such that there is no need for auxiliary energy.

B. Hooks and Jeeves

The purpose of this annex is to describe the optimization algorithm used, which is based on the Hooke and Jeeves method. The latter iteratively performs a combination of exploratory and heuristic sequence moves.

The exploratory step is repeated in the vicinity of the current point on a regular basis in order to find the best point about the current point. Then, using these two points, a pattern move in the sequence is created.

The current point is disturbed in both positive and negative directions along each variable one at a time in the exploratory move, and the best point is reported. The current point is modified to the best value at the end of any variable perturbation. If the point discovered at the end of all variable perturbations differs from the original point, the exploratory move is considered to be successful; otherwise, the exploratory move is deemed to be unsuccessful. In any case, the best point is thought to be the result of the exploratory move.

A new point is discovered by jumping from the current best point along a direction connecting the previous best point and the current base point. This phenomenon is called the pattern move. If the pattern move does not take the solution to a better region, it is rejected, and the scope of the exploratory search is reduced.

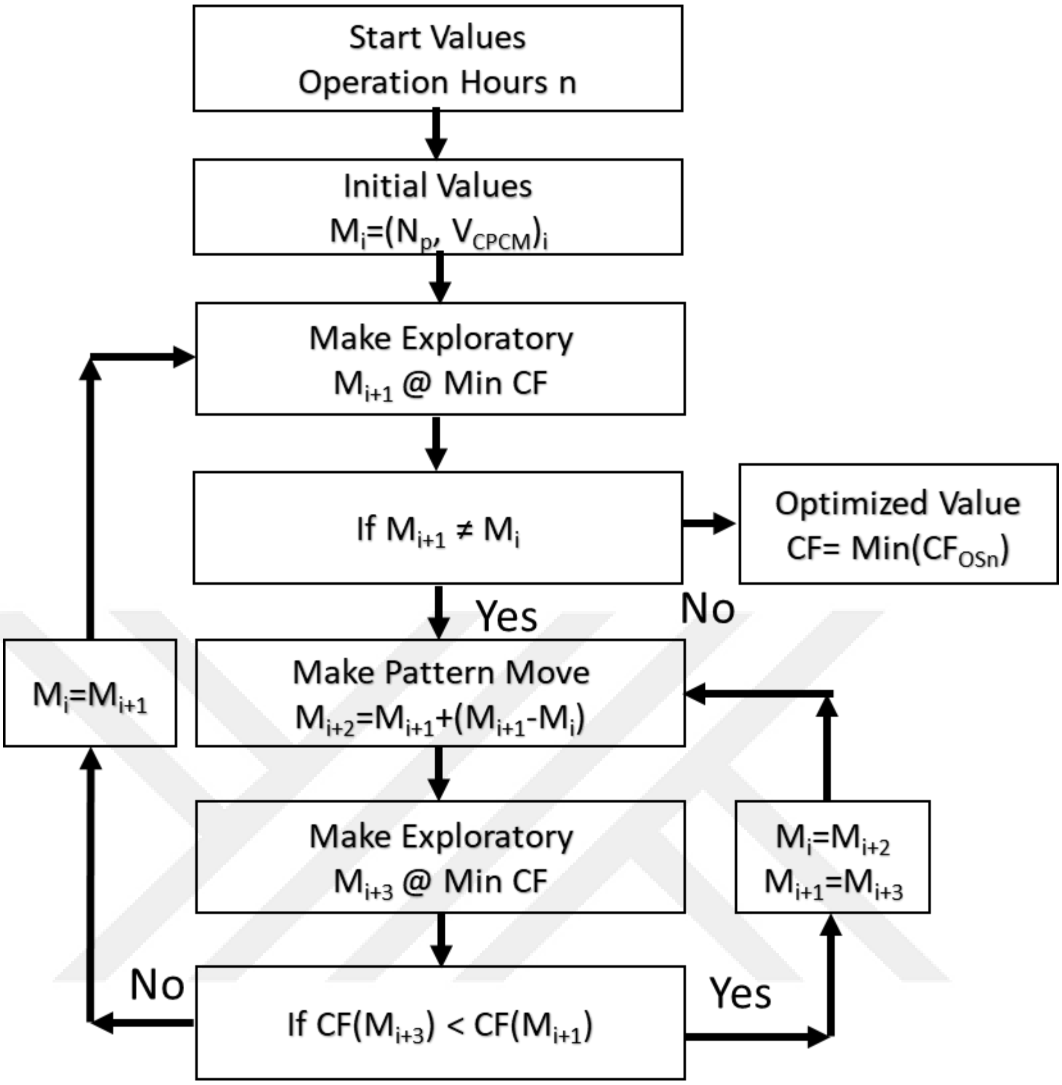

Figure 9. Optimization Algorithm Flow Chart

Step 1: Determine the Initial Point

$$N_{pi} = N_p$$

$$V_{\mathrm{CPCM}i} = V_{\mathrm{CPCM}}$$

$$CF_{\mathrm{OS}\,n} = N_{\mathrm{p}} \cdot Cost_{\mathrm{panel}} + V_{\mathrm{CPCM}} \cdot Cost_{\mathrm{CPCM}} + Cost_{VRF} + Cost_{Installation} + Pen_{(\mathrm{aux}>0)}$$

Step 2: Exploratory move along each variable one at a time

Do While k ≤ 3

$Find\ N_{\mathrm{P}(i+1)}$ @ Min { $CF_{\mathrm{OS}\,ni}(N_{\mathrm{Pi}} + step, V_{\mathrm{CPCMi}})$,

$$CF_{\mathrm{OS}ni}(N_{\mathrm{pi}} - step, V_{\mathrm{CPCMi}}),$$

$$CF_{\mathrm{OS}ni}(N_{\mathrm{pi}}, V_{\mathrm{CPCMi}})\ \}$$

Find $V_{\text{CPCM(i+1)}}$ @ Min { $CF_{\text{OS}ni}(N_{\text{p}(i+1)}, V_{\text{CPCMi}} + step)$,

$CF_{\text{OS}ni}(N_{\text{p}(i+1)}, V_{\text{CPCMi}} - step)$,

$CF_{\text{OS}ni}(N_{\text{p}(i+1)}, V_{\text{CPCMi}})$ }

$$CF_{\text{OS}n(i+1)} = N_{\text{p(i+1)}} \cdot Cost_{\text{panel}} + V_{\text{CPCM(i+1)}} \cdot Cost_{\text{CPCM}} + Cost_{\text{VRF OS}n} + Aux \cdot Pen_{(\text{aux}>0)}$$

Step 3: Check if better point is reached.

If And ($N_{\text{P}i} = N_{\text{P(i+1)}}$, $V_{\text{CPCM}i} = V_{\text{CPCM(i+1)}}$)

Then $CF_{\text{OS}ni}$ is the optimal solution

Else move to Step 4

Step 4: Pattern move;

$$N_{\text{P}(i+2)} = 2 \cdot N_{\text{P(i+1)}} - N_{\text{Pi}}$$

$$V_{\text{CPCM}(i+2)} = 2 \cdot V_{\text{CPCM(i+1)}} - V_{\text{CPCMi}}$$

Step 5: Exploratory move along each variable one at a time

Do While k $\leq$ 3

Find $N_{\text{P}(i+3)}$ @ Min { $CF_{\text{OS}n}(N_{\text{P(i+2)}} + step, V_{\text{CPCM(i+2)}})$,

$CF_{\text{OS}n}(N_{\text{P(i+2)}} - step, V_{\text{CPCM(i+2)}})$,

$CF_{\text{OS}n}(N_{\text{P(i+2)}}, V_{\text{CPCM(i+2)}})$ }

Find $V_{\text{CPCM(i+3)}}$ @ Min { $CF_{\text{OS}n}(N_{\text{P}(i+3)}, V_{\text{CPCM(i+2)}} + step)$,

$CF_{\text{OS}ni}(N_{\text{P}(i+3)}, V_{\text{CPCM(i+2)}} - step)$,

$CF_{\text{OS}ni}(N_{\text{P}(i+3)}, V_{\text{CPCM(i+2)}})$ }

$$CF_{\text{OS}n(i+3)} = N_{\text{P(i+3)}} \cdot Cost_{\text{panel}} + V_{\text{CPCM(i+3)}} \cdot Cost_{\text{CPCM}} + Cost_{\text{VRFOS}n} + Aux \cdot Pen_{(\text{aux}>0)}$$

Step 6: Check if better point is reached.

If $CF_{\text{OS}n(i+3)} \prec CF_{\text{OS}n(i+1)}$

Then

$$N_{\text{P}i} = N_{\text{P}(i+2)}$$

$$V_{\text{CPCM}i} = V_{\text{CPCM}(i+2)}$$

$$N_{\mathrm{P}(i+1)} = N_{\mathrm{P}(i+3)}$$

$$V_{\mathrm{CPCM}(i+1)} = V_{\mathrm{CPCM}(i+3)}$$

Move to Step 4

Else

$$N_{\mathrm{P}i} = N_{\mathrm{P}(i+1)}$$

$$V_{\mathrm{CPCM}i} = V_{\mathrm{CPCM}(i+1)}$$

Move to Step 2

Figure 10 displayed illustrates the implementation of the Hooke and Jeeves algorithm using the programming language Visual Basic. This code script serves as a computational framework for executing the Hooke and Jeeves optimization method, which is utilized to find the minimum or maximum of a given function.

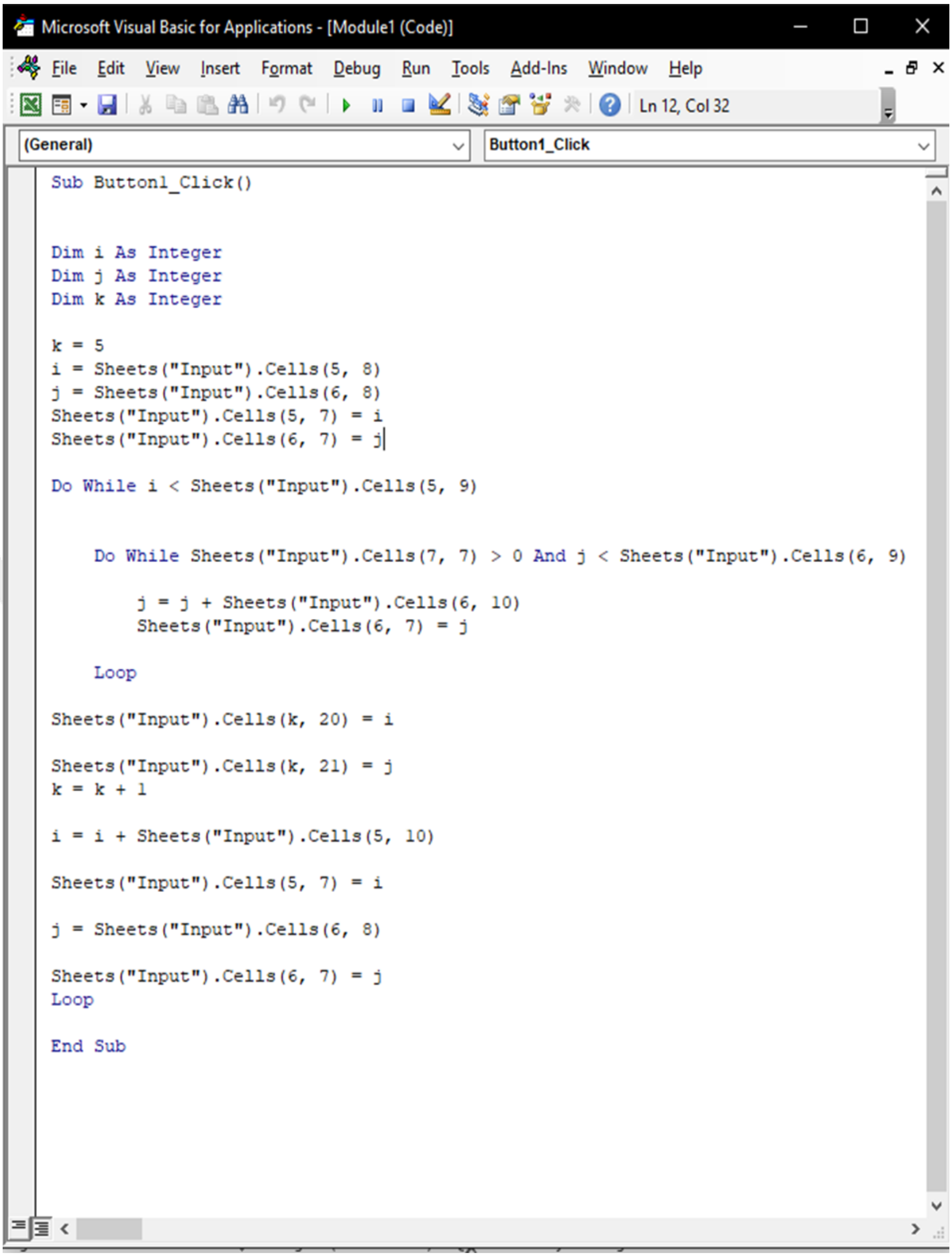

Figure 10. Hooke and Jeeves code using Visual Basic

C. Electro/Thermo-Economical Optimization

Thus, the optimization method used for this project is considered an Electro- economical optimization that consists of getting the optimal result based on the cost of the project. It's about finding the minimal required equipment that could guarantee the customer the full autonomy of the system.

In this case, the two systems are considered separately. For the PV-Batteries system, the hourly cooling load was compared to the PV-Electrical Energy. When the PV's electrical energy is higher than the required cooling load, the batteries are charging. However, when the cooling load required by the building is higher than the energy supplied by the PV system, the batteries will help the Photovoltaic panels to achieve the required level. In order to proceed to achieve this result, one variable, which is the number of panels, shall be fixed, and the other variable, which is the charge capacity of the batteries will be incremented.

For the PV-PCM cold storage system, the hourly cooling load was compared to the Thermal Energy produced (available) from the VRF system. When this thermal energy is higher than the required cooling load, the PCM cold storage is charging. However, when the cooling load required by the building is higher than the thermal energy supplied by the VRF system, the storage will help the Photovoltaic panels to achieve the required level. In order to proceed to achieve this result, one variable, which is the number of panels, shall be fixed, and the other variable, which is the cold PCM capacity will be incremented.

Increasing the number of panels of batteries/cold PCM beyond the needs will result in oversizing the system and this will affect the cost of our system, this is why, there is a certain number of panels that meets the minimum needed loads, and this number should be picked for our system. A minimal and maximal value for the variables should be considered depending on the circumstances of the project.

ANNEX. 2 DESIGN BUILDER

This annex serves the purpose of showcasing the model, inputs, and resulting data that can be generated using the "Design Builder" tool. Within the program, Figure 11 depicts the villa's model as it was built. Additionally, Figures 12 and 13 provide an overview of the distinct zones and spaces located on the ground and first floors of the villa.

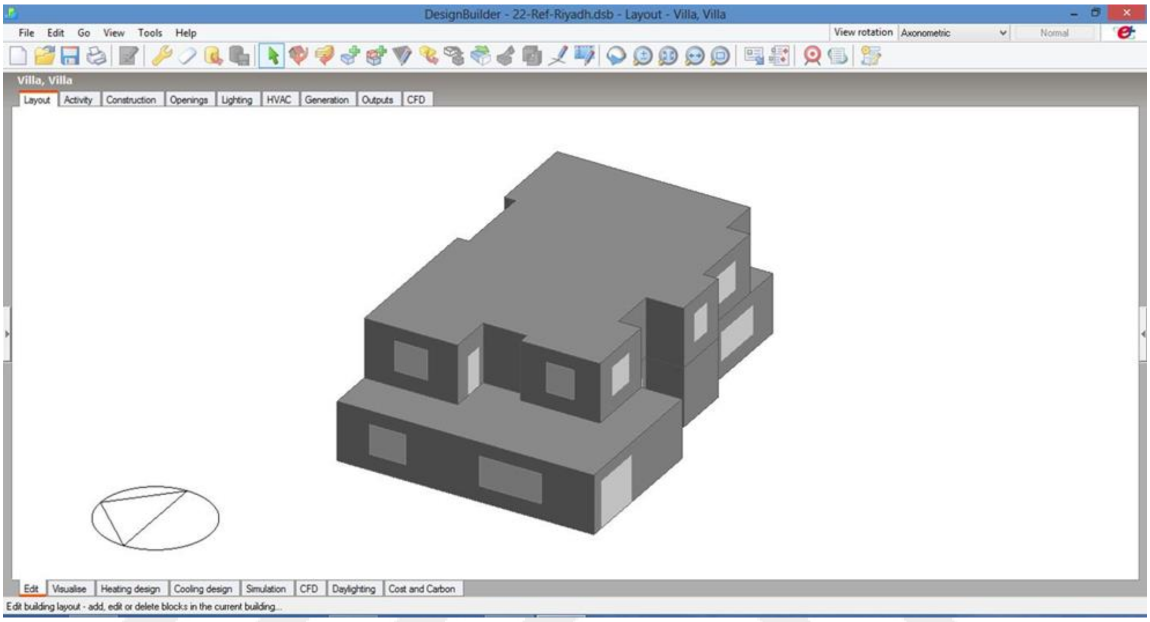

Figure 11. Villa's Model

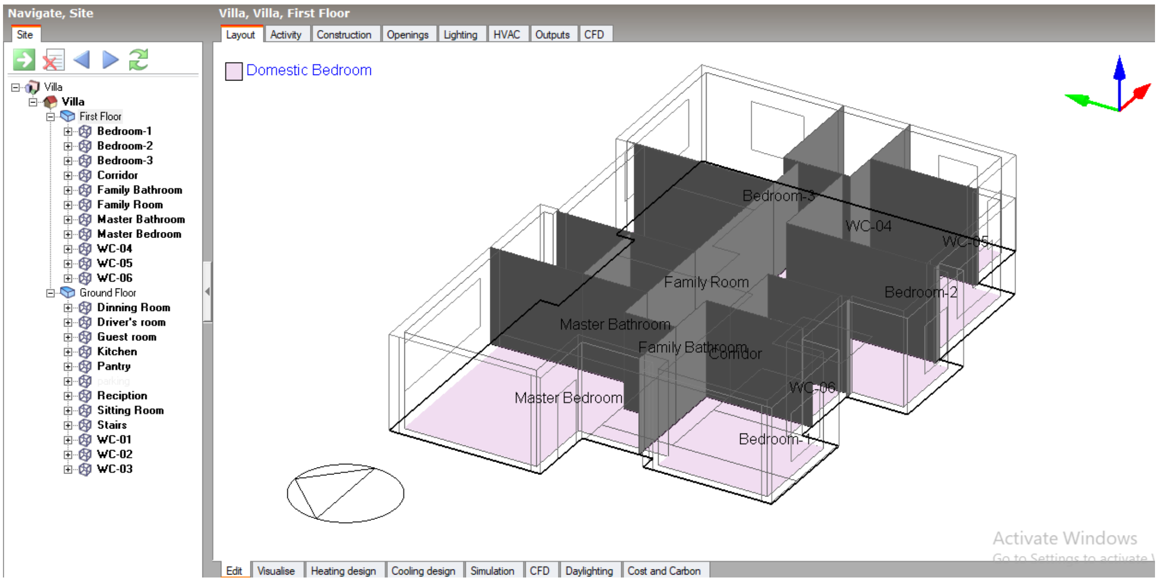

Figure 12. First floor zones

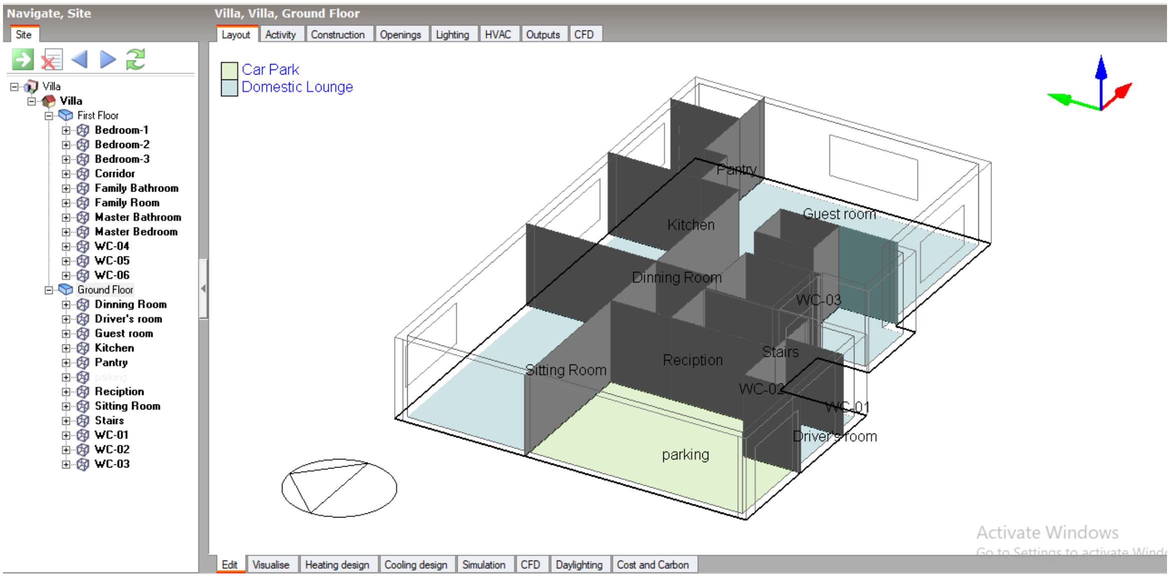

Figure 13. Ground floor zones

Figures 14 and 15 demonstrate various constructional inputs that can be incorporated into the Design-Builder, such as walls, ceilings, windows, and shading. Meanwhile, Figure 16 displays the resulting thermal energy consumption data in sub-hourly intervals.

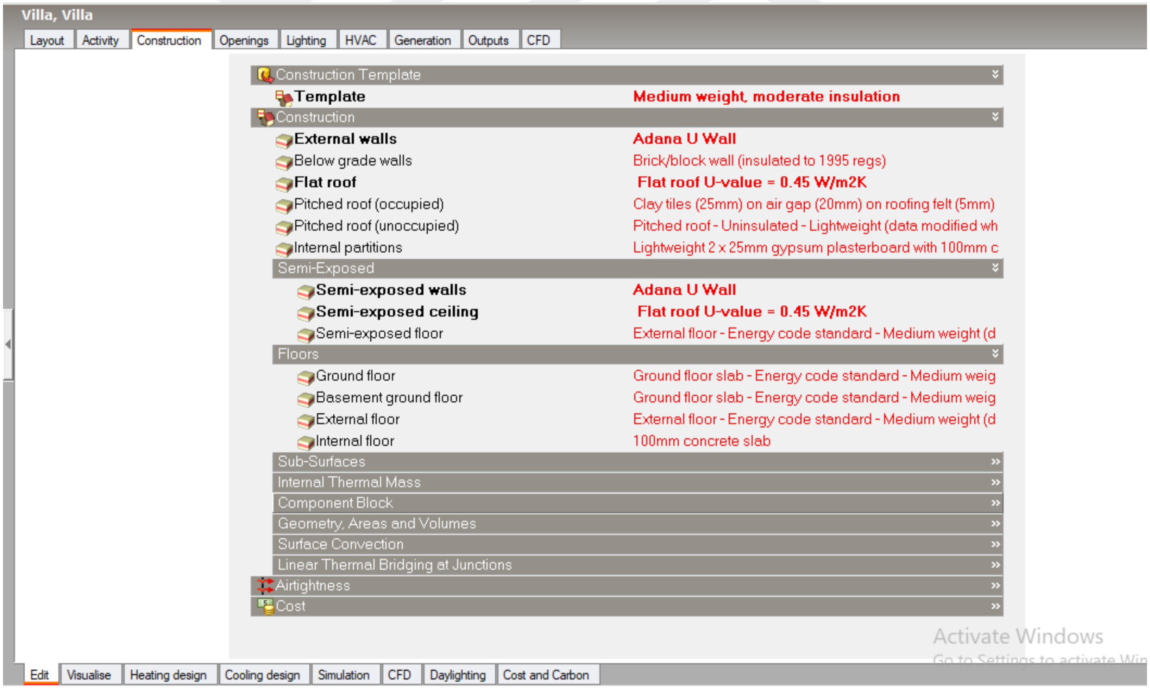

Figure 14. Construction Input Values

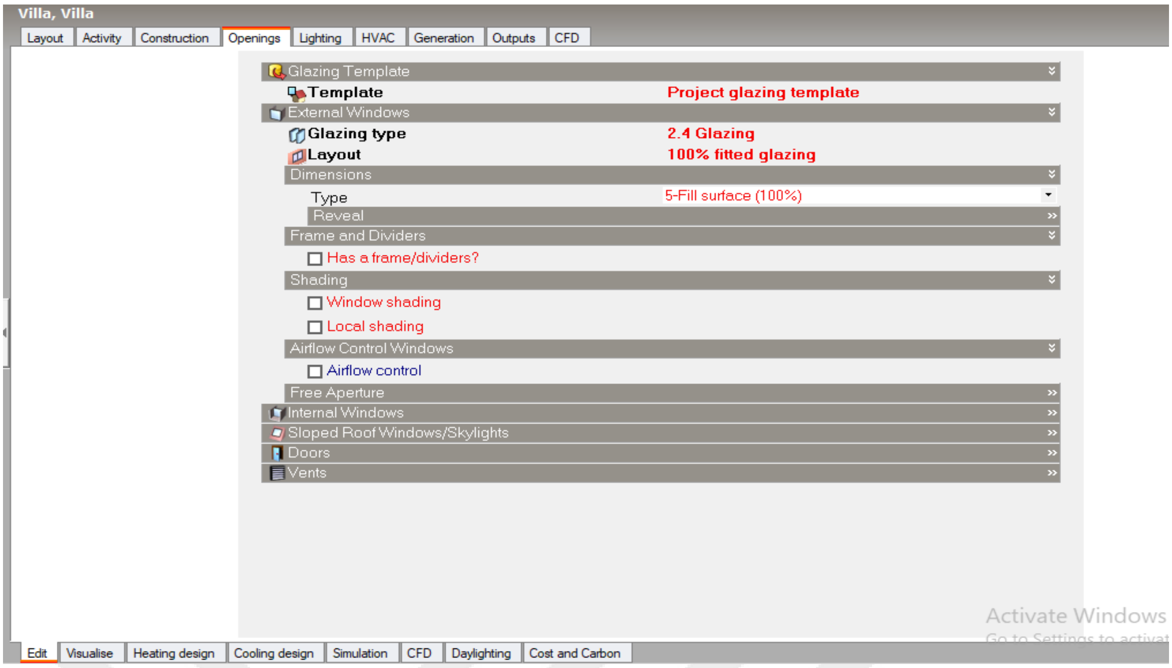

Figure 15. Glazing Input Values

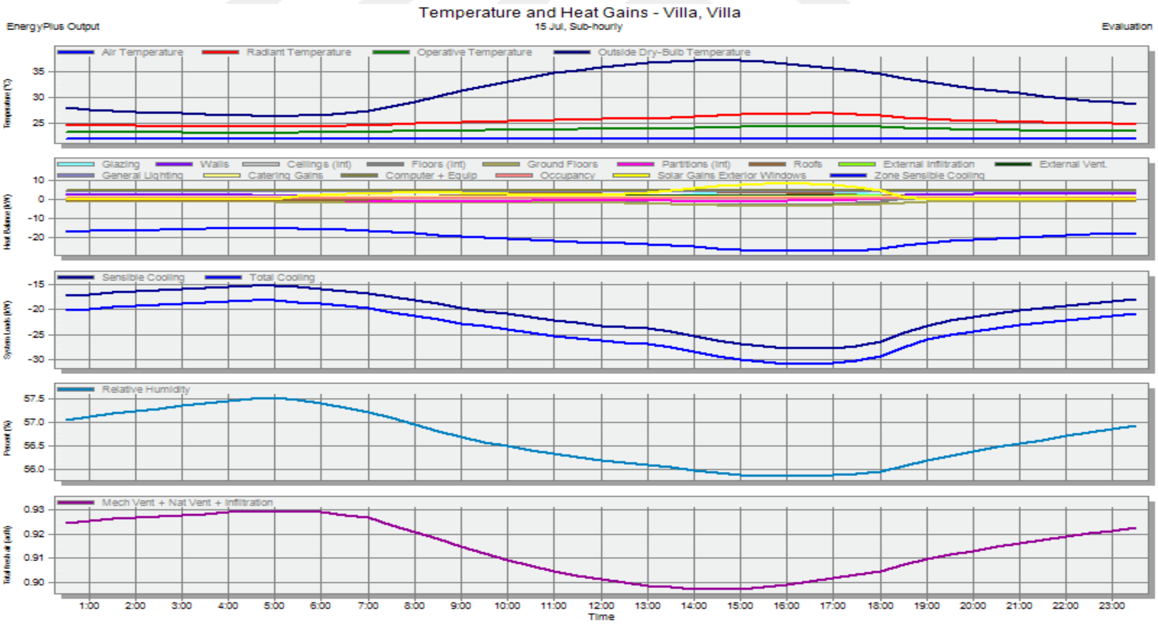

Figure 16. Sub-hourly Energy Consumption